Counterions, smectite, and palygorskite increase microstructural stability of saline-sodic soils

Article published in Soil & Tillage Research
https://doi.org/10.1016/j.still.2021.105258

Authors:

F. Javaheri
Ph.D. student of Soil Science and Engineering Department, College of Agriculture,
Vali-e-Asr University of Rafsanjan, Rafsanjan, Iran
Email: f.j.active@gmail.com

I. Esfandiarpour-Boroujeni
Associate prof. of Soil Science and Engineering Department, Faculty of Agriculture,
Vali-e-Asr University of Rafsanjan, Rafsanjan, Iran
Email: esfandiarpoor@vru.ac.ir

M. H. Farpoor
Professor of Soil Science Department, Faculty of Agriculture,
Shahid Bahonar University of Kerman, Kerman, Iran
Email: farpoor@uk.ac.ir

Dörthe Holthusen
Post-doctoral researcher, Department of Vegetation Studies, Landscape Management, Federal Institute of Hydrology, Koblenz, Germany.
Email: Holthusen@bafg.de

R. D. Stewart
Associate prof. of Plant and Environmental Sciences Department, Faculty of Environment,
Virginia Tech. University, Blacksburg, VA, USA
Email: ryan.stewart@vt.edu

Corresponding Author:

I. Esfandiarpour-Boroujeni
Associate prof. of Soil Science and Engineering Department, Faculty of Agriculture,
Vali-e-Asr University of Rafsanjan, Rafsanjan, Iran
Email: esfandiarpoor@vru.ac.ir

Highlights

- Microstructural stability of saline-sodic soils in Sirjan Playa were analyzed via rheometry.
- Sodium content had negative, non-significantly correlation with microstructural stability.
- Smectite, palygosrkite, gypsum, and calcium carbonates increased microstructural stability.
- Samples with negative matric potentials increased microstructural stability similarly.
- Soil texture, mineralogy, and counterion concentrations may also translate to mesoscale considerations of erosion assessment.

Abstract

Saline-sodic soils are susceptible to wind and water erosion when the dispersive effect of sodium overcomes inter-particle bonds. Rheological parameters of viscoelasticity can help to quantify inter-particle attractive forces and account for the effect of salinity in these soils. The main objective of the present study was to investigate the viscoelasticity behavior of saline-sodic soils of the Sirjan playa in south-central Iran. Three representative pedons were excavated and described by horizon. Soil physicochemical properties and rheological properties were determined, namely the micromechanical parameters flow point (γ_f), loss factor tan δ, and *integral z*, with samples analyzed at three matric potentials (0, −6, and −15 kPa). Results showed that soil microstructural stiffness was mainly influenced by soil texture, clay minerals, gypsum, calcium carbonate equivalent (CCE), and matric potential. The dispersive effect of sodium, as indicated by low *integral z* and γ_f values, decreased with increasing gypsum content in − 6 and − 15 kPa matric potentials ($0.6 < r < 0.8$) and CCE percentage in the quasi-saturated (0 kPa) condition ($r > 0.8$). However, greater microstructural stability (i.e., higher *integral z* and γ_f) was observed for fine-textured soils with relatively high amounts of smectite and palygorskite and low pH. Furthermore, *integral z* and γ_f increased with lower matric potentials due to the stabilizing effect of menisci forces. Therefore, the viscoelastic behavior of the saline-sodic soils was negatively associated with water content and high sodium concentration, while the presence of smectite, palygorskite, gypsum, and CCE improved the soil physical conditions and thus the rigidity of the porous system. These results demonstrate that rheological measurements can identify saline-sodic soils that have strongly degraded microstructural stability and would most benefit from active management and amelioration.

Keywords

Rheology

Soil viscoelastic behavior

Clay minerals

Matric potential

Soil dispersion

Sirjan Playa, Iran

1. Introduction

Saline-sodic playas exist in many arid and semi-arid inland areas. The main requirement for the formation of these landscapes is that annual evaporation exceeds annual precipitation (Smith, 1977, Han et al., 2019). Capillary rise from shallow groundwater (i.e., 0.01 to ~1 m below the soil surface) can lead to superficial salt crust formation because of the continuous supply of water and dissolved salts (Han et al., 2019). In general, saline-sodic soils exhibit poor structural stability, salt crust formation, dispersion, slaking, and hard-setting, which can reduce the rates of water and gas movement (Qadir and Schubert, 2002, Qadir et al., 2006), and make soil particles susceptible to wind and water erosion due to poor physical structure (Agassi et al., 1981, Qadir et al., 2006).

Many of these problems arise during clay swelling and dispersion processes (Reading et al., 2012), which depend on mineral properties such as surface electrical characteristics (Holthusen et al., 2020, Ni and Huang, 2020). For instance, smectite and vermiculite particles have moderate to high swelling ability as they attract hydrated cations and water molecules to their interlayer spaces. These same electrostatic interactions often lead swelling clays to better resist deformation than non-swelling minerals such as kaolinite (West et al., 2004; Markgraf et al., 2007) and illite (Suarez, 1981, Oster, 1982). Nonetheless, swelling clays differ in their tendency to disperse, depending on factors like the rate of mineral dissolution (with faster dissolving particles having less stability), the ability of soils to release salts during leaching (with faster salt release rates associated with lesser tendency to disperse), and the shear resistance of the mineral phase (with higher shear restistance associated with more stability; Shainberg et al., 1981; Torrance, 1999; Holthusen et al., 2010). At the same time, non-swelling minerals with fibrous structures, including palygorskite and sepiolite, have moderate internal charge and tend to be highly stable when in suspension (Fuchs, 2005), meaning that their presence may increase soil microstructural stability.

The bulk electrolyte concentration of the soil solution also influences interactions between soil particles (e.g., DLVO theory; Adamczyk and Weroński, 1999; Missana and Adell, 2000). In particular, the concentration and type(s) of soluble salt present in the soil solution affects the inter-layer expansion of smectite and vermiculite (Swenson et al., 2002, Batistao et al., 2020, Ni and Huang, 2020). Soil dispersion primarily occurs when monovalent sodium replacements divalent “bridging” cations such as calcium and magnesium, which increases the zeta potential and encourages particles to detach from one another (Quirk and Murray, 1991). Inter-particle swelling can then act to further disperse the particles, causing the clogging of larger soil pores and reducing hydraulic conductivity (Markgraf et al., 2012a, Reading et al., 2012). However, these dispersive processes diminish as sodium concentration increases (e.g., > 3% concentration; DeCarlo and Shokri, 2014). Only a few studies have analyzed the relationships between clay mineral composition and viscoelasticity of soils with high levels of salinity and sodicity (Stoppe and Horn, 2018, Ni and Huang, 2020), meaning that there is limited understanding of the factors that enhance versus resist dispersion in saline-sodic soils.

In order to evaluate the likelihood of saline-sodic soils becoming dispersed and eroded, it is important to understand the circumstances under which the soil microstructure remains intact (i.e., experiences reversible strain) versus becomes irreversibly altered. Considering and

characterizing soils as viscoelastic substances can help in this regard (e.g., Ni and Huang, 2020). Viscoelastic substances experience both elastic (reversible) and viscous or plastic (irreversible) deformation upon shearing, and the relative proportion of each of these behaviors indicates shifts and destruction of microstructural arrangements of particles (Ghezzehei and Or, 2001, Markgraf et al., 2006). Rheometric measurements such as amplitude sweep tests (AST) characterize viscoelastic behaviors of soils, and thereby offer the possibility to evaluate soil reactions to transient stresses and distinguish different types of bonds (e.g., resilient or unrecoverable bonds; Holthusen et al., 2019 and 2020). In recent years, rheometry has been used to improve the understanding of microscale processes in many soils (Torrance, 1999, Ghezzehei and Or, 2001, Markgraf et al., 2009, Holthusen et al., 2010, Stoppe and Horn, 2018, Khitrov and Khaydapova, 2019, Javaheri et al., 2021). However, most studies have been conducted in humid or arable regions, with relatively few studies looking at salt-affected, arid soils (e.g., Markgraf et al., 2012a; Stoppe and Horn, 2018).

The Sirjan area of Kerman Province, south-central Iran, is an arid region containing many pistachio orchards. Because many soils in the area are affected by salts from the nearby Sirjan Playa, growers there must deal with challenges such as low infiltration rates and hardpan formation from carbonate accumulation (Farpoor et al., 2012). Proper management of such salt-affected croplands requires better understanding of the factors that influence soil microstructural stability. Therefore, in this study we compared rheological properties of three saline-sodic soil profiles surrounding the Sirjan playa. Our main objectives were to: (i) calculate the quasi-elasticity parameters *integral z*, which quantifies microstructural stability across a range of stresses, for the saline-sodic soils of the Sirjan play, and γ_f, which represents the deformation required for the soil to become viscous; (ii) determine how physicochemical properties and clay mineral composition affect the shear behavior and stiffness degradation of these soils under oscillatory stress conditions; and (iii) specify the influence of dewatering by means of performing the tests under three different matric potentials: 0, − 6, and − 15 kPa.

2. Materials and methods

2.1. Study area

Sirjan Playa (29° 20′−29° 30′ N and 55° 30′−55° 40′ E) is located in the Kerman Province, south-central Iran, and has a total area of 1625 km^2 (Fig. 1). Sirjan Playa is the remnant of a large ancient lake (Farpoor et al., 2012), and is surrounded by alluvial plains that were created by joining alluvial fans. The area has a mean elevation of 1650 m a.s.l. and an arid climate (Köppen-Geiger climate classification system; Kottek et al., 2006). It has a mean annual temperature of 17.3 °C and a mean precipitation of 133.3 mm. The area has an aridic/aquic soil moisture regime and thermic temperature (Farpoor et al., 2012). The drainage system of the playa is often active during seasonal floods and it is generally dry for the rest of the year. Pistachios are the main crop grown in the area, with most trees located at or beyond the western margin of the playa due to better soil conditions (e.g., lower soil strength, less erosion) and greater water availability.


Caspian Sea
Turkmanistan
Iraq
Tehran
Afghanistan
Kuwait
Kerman
Saudi Arabia
Persian Gulf
Oman Sea
0 80 160 240 Km


Kerman
Sirjan
0 70 140 210 Km


340000
360000
3260000
3240000
P3
P2
P1
Sirjan
Sirjan Playa
Goad-Ghool Mountains
Kaviz Mountains
0 5 10 15 Km

1. Download : Download high-res image (2MB)
2. Download : Download full-size image

Fig. 1. Location of the study area (top) and the representative pedons (bottom).

2.2. Soil sampling and laboratory analyses

To study the viscoelastic behavior of saline-sodic soils of the playa, we excavated three representative pedons on different geomorphic surfaces, i.e., the playa margin (Pedon 1: P1), a wet zone (Pedon 2: P2), and a clay flat with the puffy ground (Pedon 3: P3). We selected pedons on the margins of the Sirjan Playa, rather than in the playa interior, for several reasons. For one, these locations were more accessible, i.e., within reach of roads, and sampling was not hindered by the presence of seasonal ponding. For another, the selected pedons were more representative of agricultural soils in the area. At the same time, the three pedons formed a transect, with elevations of 1700 m (P1), 1690 m (P2), and 1680 m (P3) above sea level (Fig. 1). In terms of vegetation, P1 was located near some pistachio orchards and had a sparse vegetative cover of shrubs and small trees, while P2 and P3 were barren. The pedons were described according to Schoeneberger et al. (2012), and were classified using the WRB system IUSS Working Group WRB (2015). The three pedons are shown in Fig. 2.

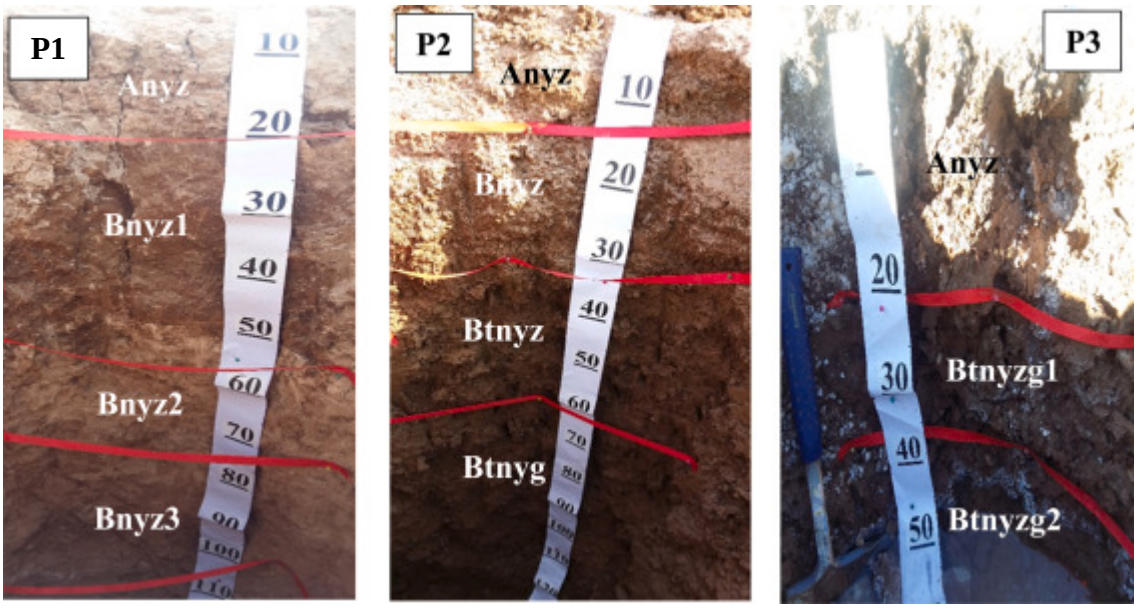

1. Download : Download high-res image (880KB)
2. Download : Download full-size image

Fig. 2. View of the studied pedons (P1 = Pedon 1; P2 = Pedon 2; P3 = Pedon 3).

Soil samples were taken from different genetic horizons of the pedons and transferred to the laboratory. There, all samples were air-dried and passed through a 2-mm sieve. Analyzed physicochemical properties (n = 3) included the percentage of the coarse fragments by sieving,

particle size distribution by the pipette method (Gee and Bauder, 1986), and pH of saturated paste using a Jenway pH meter at 25 °C. Calcium carbonate equivalent (CCE) was investigated using the HCl back-titration method (Nelson and Summers, 1982) and gypsum was expressed as a % (i.e., g/100 g soil) using an acetone-based method (Richards, 1954). Cation exchange capacity (CEC) was measured by NH_4OAc at pH 7.0 (Sumner and Miller, 1996), and soluble cations – including Mg^{2+}, Ca^{2+}, Na^{+}, and K^{+} – were measured in a saturated extract using GBC SAvantAA atomic absorption spectrophotometry and flame photometry (Rayment and Higginson, 1992). Electrical conductivity (EC) was measured in a saturated paste using an Jenway EC meter (Cole-Parmer, Staffordshire, UK) at 25 °C. The sodium adsorption ratio (SAR) was calculated following Richards (1954) as:(1)

where Na^{+}, Ca^{2+}, and Mg^{2+} concentrations in the soil solution in $mmol_c\ L^{-1}$. However, some saline-sodic soils have a high potassium concentration; hence, this cation may need to be considered as well. Therefore, we also calculated the cation ratio of soil structural stability (CROSS) according to Rengasamy and Marchuk (2011):(2)

where the concentrations of the cations are expressed in $mmol_c\ L^{-1}$.

We analyzed samples from four of the thirteen genetic horizons for clay mineralogical analysis. Specifically, we analyzed the Bnyz1 horizon of P1, the Anyz and Btnyz horizons of P2, and the Btnyzg2 horizon of P3 (Table 1). The A horizon sample came from 10 cm deep, while the B horizon samples came from 40 cm deep, thus representing the same depth of different genetic horizons. For the X-ray analysis, four saturation treatments were applied for clay fraction samples, including saturation with Mg (using 1 N $MgCl_2$), Mg and ethylene glycol (using a desiccator containing ethylene glycol and saturated sample with Mg), K (using 1 N KCl), and K and 550 °C (using a thermal furnace for two hours), following the procedures of Jackson (1958) and Kittrick and Hope (1963). Then, the samples were analyzed using a Bruker D8 advanced X-ray diffractometer equipped with CuKα radiation (λ = 0.15418 nm) operating at a tube current of 40 mA and a voltage of 40 kV. Samples were scanned from 4° to 40° 2θ. The identification of clay minerals was done by comparing the diffractograms following the Dixon and Weed (1989) guideline.

Table 1. Summary of morphological properties of the studied pedons. - = Not detected. ⸸ indicates soil horizons that were analyzed for mineralogy; * indicates soil horizons that were analyzed using the amplitude sweep tests for rheological properties.

Pedon No.	Horizon	Depth (cm)	Boundary[a]	Color		Consistency[b]		SR[c]		Mottles[d]/ Redoximorphic features[e]
				Dry	Moist	Dry	Moist			
Pedon 1: Gypsic Sodic Solonchacks										
1	Anz*	0–21	–	10 YR 5/4	10 YR 4/6	HA	L		pl	–

Pedon No.	Horizon	Depth (cm)	Boundary[a]	Color		Consistency[b]		SR[c]	Mottles[d]/ Redoximorphic features[e]
				Dry	Moist	Dry	Moist		
	Bnyz1 *	21–52	V-W	7.5 YR 4/3	7.5 YR 3/3	VH	FI	abk	–
	Bnyz2	52–73	V-W	10 YR 6/3	7.5 YR 4/3	SH	VFR	abk	–
	Bnyz3	73–97	C-S	10 YR 6/4	7.5 YR 4/4	MH	FR	abk	–
	Bnyz4	97–132	C-S	10 YR 6.5/3	7.5 YR 3/2	MH	FR	abk	–
Pedon 2: Gypsic Salic Gleyic Solonetz									
2	Anyz*	0–12	–	7.5 YR 4/3	10 YR 5/6	L	L	pl	–
	Bnyz	12–32	A-W	7.5 YR 3/3	7.5 YR 4/3	L	L	sbk	–
	Btnyz*	32–61	C-S	10 YR 6/3	7.5 YR 3/3	HA	FR	cpr	c, 1, D, 10 Y 6/1, M, S
	Btnyg	61–130	C-S	10 YR 6/3	7.5 YR 3/2	VH	SO	cpr	m, 4, P, 10 Y 6/1, M, SRMX, c, 2, D, 10 Y 6/1, M, I, MAT, L, S
Pedon 3: Gypsic Salic Solonetz									
3	Anz*	0–21	–	10 YR 5/3	10 YR 2/2	L	L	pl	–

Pedon No.	Horizon	Depth (cm)	Boundary[a]	Color		Consistency[b]		SR[c]	Mottles[d]/ Redoximorphic features[e]
				Dry	Moist	Dry	Moist		
	Btnyzg1	21–38	A-W	10 YR 6/3	7.5 YR 3/2	VH	SS	cpr	c, 2, D, 5GY 5/1, M, S
	Btnyzg2 *	38–62	C-S	10 YR 6/3	7.5 YR 3/2	VH	SS	cpr	m, 2, P, 5GY 5/1, M, S
	Bzm	62 +	C-S	–	–	EH	–	–	–

a

Boundary: very abrupt (V), abrupt (A), clear (C), smooth (S), wavy (W)

b

Consistency: Dry: loose (L), slightly hard (SH), moderately hard (MH), hard (HA), very hard (VH), extremely hard (EH); moist: loose (L), very friable (VFR), friable (FR), firm (FI), slightly sticky (SS), non-sticky (SO)

c

Soil structure (SR): angular blocky (abk), subangular blocky (sbk), platy (pl), columnar (cpr)

d

Mottles: common (c), m (many), fine (1), medium (2), very coarse (4), distinct (D), prominent (P), moist (M), spherical (S)

e

Redoximorphic features: reduced matrix (RMX), common (c), medium (2), distinct (D), moist (M), irregular (I), in the matrix (not associated with peds/pores) (MAT), loose (L), sharp (S)

2.2.1. Rheometry analyses

Also due to limited laboratory access and funding constraints, we analyzed rheological properties for a subset of six (out of thirteen) of the genetic horizons. We selected soil samples from the Anz and Bnyz1 horizons in P1, the Anyz and Btnyz horizons in P2, and the Anz and Btnyzg2 horizons in P3 (Table 1). As in the mineralogical analysis, the A horizon samples were collected

at 10 cm depth and the B horizon samples were collected at 40 cm depth. The soils were sieved through a 2-mm mesh and repacked to a standard bulk density (1.3 g cm^{-3}) within 45 cm^3 cylinders. We used a bulk density of 1.3 g cm^{-3} to have a uniform value for all samples, in agreement with previous studies (Baumgarten, 2013, Ajayi and Horn, 2017, Liu et al., 2017).

Three samples from each horizon were capillary saturated with distilled water, with 0 kPa at the bottom (contact of the cylinder to the water table). A small amount of soil was taken out of each cylinder with a spatula and put on the measuring plate of a Discovery Hybrid Rheometer-3 (DHR-3, TA Instruments, New Castle, DE, USA), equipped with a parallel-plate measuring system that was 25 mm in diameter at a plate distance of 4 mm (Markgraf and Horn, 2007). Amplitude sweep tests (AST) with controlled shear deformation (CSD, logarithmic ramp of $\gamma = 0.0001–100\%$) under oscillatory conditions were performed at 25 °C with the frequency was set at a constant value of $f = 0.5$ Hz (angular frequency, $\omega = \pi s^{-1}$). The normal force on the sample did not exceed 14 N at the beginning of the test and approximated 0 N by the end of the test (Baumgarten et al., 2012). Tests were completed within 8–10 min, which ensured that the edges of the samples did not dry.

Once the tests were completed on the quasi-saturated samples, the cores were placed on pressure plates and equilibrated to − 6 kPa matric potential. The AST procedure was repeated. Then, the samples were equilibrated to − 15 kPa matric potential, and a final AST analysis was performed. Three replicates were used for each combination of soil horizon and matric potential (i.e., 0, −6, −15 kPa).

2.2.2. Loss factor tan δ and integral z

The oscillating movement of the upper plate in an AST causes oscillating stress reactions of the soil; however, the peak amplitudes become delayed due to the viscous portion of soil deformation (Mezger, 2006). This delay is represented by the phase shift angle δ and its tangent, tan δ. The more pronounced the delay, the more viscous (plastic) the soil is, which is reflected by increasing δ and tan δ (Markgraf et al., 2006). A soil sample experiences a gradual degradation of microstructural stiffness, as represented by tan δ, during the AST (Fig. 3). The elastic and plastic/viscous deformation of material are respectively represented by storage and loss moduli, G′ and G″ (Markgraf et al., 2006), and the ratio of these two moduli are equivalent to the loss factor, tan δ.

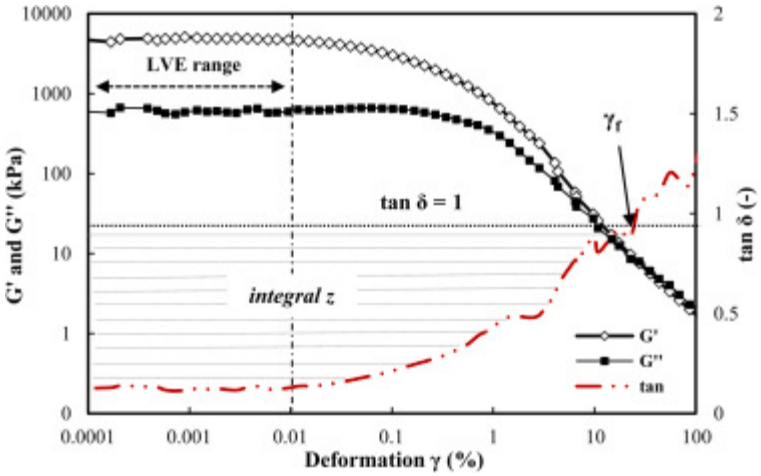

1. Download : Download high-res image (283KB)
2. Download : Download full-size image

Fig. 3. Example of an amplitude sweep test (AST) result showing G′ (storage modulus) and G″ (loss modulus) as functions of deformation, γ. The loss factor, tan δ, equals

. The *integral z* parameter is calculated as the area between tan δ and 1. The quasi-elastic stage is defined by the linear viscoelastic (LVE) range and derived deformation limit (vertical dashed line). The transition phase between elastic and viscous deformation occurs between the deformation limit and the flow point (γf).

Within the linear viscoelastic range (LVE), G′ and G″ remain approximately constant with increasing applied shear strain, indicating fully reversible deformation.Beyond the deformation limit (γ_L), the soil enters the transgression phase, in which G′ and G″ both decline with increasing deformation and tan δ increases as the deformation becomes increasingly viscous. When tan δ = 1, the flow point (γ_f) is reached and the materials enter the final stage of structural collapse (Pertile et al., 2018). In this final phase, tan δ > 1 and viscous behavior predominates, resulting in microstructure collapse and irreversible failure (Markgraf and Horn, 2007, Mezger, 2020).

In order to compare quasi-elastic behavior under prevailing elastic deformation (i.e., tan δ < 1), we used the dimensionless parameter *integral z* (Stoppe and Horn, 2018):(3)

We assumed that tan δ measured at deformation= 0.001% was representative of initial values for that parameter (i.e., at no deformation). The TRIOS/v5.1.0 software program (TA, USA) and MATLAB/v8.1.347 were used to calculate the γ_f and *integral z* parameters.

3. Results

3.1. General soil properties

P1 was classified as a Gypsic Sodic Solonchack, and P2 and P3 were classified as Gypsic Salic Solonetz, with P2 also having gleyic properties (Table 1). Solonchacks and Solonetz are two

reference soil groups, as their formation requires an abundant presences of salts and high evaporation conditions. Solonchacks and Solonetz soils are typically dense and hard when dry. However, they tend to become sticky up to viscous once wet, and can lose their bearing capacity at higher soil water contents (Krinsley, 1970, Farpoor et al., 2012).

In terms of morphological indicators, all pedons had the platy structure in their surface A horizons, while the B horizons had subangular blocky and columnar structures (Table 1). The soils of P2 and P3 were characterized by mottles and hydromorphic features such as reduced grey features, likely the result of waterlogging. Besides, the existence of the shallow water-table conditions and gleyic properties were visually observed in the Solonetz soils with a network of cracks, i.e. polygons, on their surface when dry.

The studied pedons also varied in their physicochemical properties (Table 2). For example, soil texture ranged from clay (in the subsurface horizons of P2) to sandy loam (in the subsurface horizons of P1). The soils had high salinity, with EC from 33 to 347 dS m^{-1}, and high sodicity, with SAR from 75 to 456 (mmol L^{-1})$^{0.5}$. The SAR value was lowest in the Anz horizon of P1, while the highest SAR value was observed in the Bnyz3 horizon of P1. Those same trends also appeared in the CROSS values. The SAR and CROSS metrics both indicated considerable enrichment of sodium in these soils, even in horizons with relatively low values. These soils therefore likely have low structural stability and a high probability of dispersion.

Table 2. Summary of physicochemical properties of the studied pedons.

Horizon	Depth (cm)	Clay	Sand	CF	CCE	Gypsum	CEC ($cmol_{(+)}$ kg^{-1})	pH	EC (dS m^{-1})	SAR (mmol L^{-1})$^{0.5}$	CROSS (mmol L^{-1})$^{0.5}$	ST
				(%)								
Pedon 1												
Anz	0–21	18.3	51.0	30.0	9.3	14.6	7.9	7.47	33	75	86	L
Bnyz1	21–52	19.3	58.0	12.4	11.5	16.4	8.3	7.43	48	156	174	SL
Bnyz2	52–73	20.7	64.7	11.9	7.6	26.4	8.6	7.67	70	216	229	SCL
Bnyz3	73–97	17.0	73.0	10.0	7.4	23.2	6.7	7.70	170	456	488	SL
Bnyz4	97–132	14.7	80.7	8.0	7.2	12.5	6.3	7.83	56	232	258	SL
Pedon 2												
Anyz	0–12	25	18.3	5.2	7.5	6.2	19.2	6.71	173	355	393	SiL
Bnyz	12–32	30.7	24.1	2.0	9.4	18.7	23.7	6.83	60	282	335	CL

Horizon	Depth (cm)	Clay	Sand	CF	CCE	Gypsum	CEC ($cmol_{(+)}$ kg^{-1})	pH	EC (dS m^{-1})	SAR (mmol $L^{-1})^{0.5}$	CROSS (mmol $L^{-1})^{0.5}$	ST
		(%)										
Btnyz	32–61	50.0	22.0	0.0	9.5	24.3	26.2	6.80	31	113	136	C
Btnyg	61–130	47.7	13.1	0.0	11.5	21.4	21.2	6.88	29	143	164	C
						Pedon 3						
Anz	0–21	26.3	44.8	0.0	7.5	14.8	18.7	6.53	220	167	186	L
Btnyzg1	21–38	35.3	40.8	0.0	8.0	17.9	20.4	6.40	317	243	272	CL
Btnyzg2	38–62	38.0	35.0	0.0	8.3	17.9	20.8	6.49	347	271	300	CL
Bzm	62 +	–	–	–	–	–	–	–	–	–	–	–

CF = Coarse fragments; CCE = calcium carbonate equivalent; CEC = cation exchange capacity (cmol(+) kg-1); SP = saturation percentage; EC = electrical conductivity (dS m-1); OP = osmotic potential; SAR = sodium adsorption ratio; CROSS = cation ratio of structural stability. ST = soil texture, and C = Clay, L = Loam, CL = Clay Loam, SL = Sandy Loam, SiL = Silt Loam, SCL = Sandy Clay Loam. - = Not detected.

The soil horizons at P1 had the lowest CEC values (6.3–8.6 $cmol_{(+)}$ kg^{-1}), whereas the Btnyz horizon of P2 had the highest CEC (26.2 $cmol_{(+)}$ kg^{-1}). The CCE and gypsum contents were different between pedons and horizons, the former ranging from 7.2% in the Bnyz4 horizon of P1 to 11.5% in the Btnyg horizon of P2 and the latter varying from 6.2% in the Anyz horizon of P2 to 26.4% in the Bnyz2 horizon of P1. Soil pH ranged from slightly acidic to slightly alkaline.

3.2. Clay minerals

Smectite, illite, vermiculite, palygorskite, chlorite, and kaolinite in the clay fraction were identified in the samples in moderate (10–25%) to dominant (>25%) amounts (Fig. 4). The 0.71 nm (001) and 0.35 nm (002) reflections indicated the presence of minor quantities of kaolinite, while quartz was indicated by peaks at 0.42 and 0.33 nm. The 1.43 nm (001) asymmetric peaks on the X-ray diffraction of the Mg-saturated treatment indicated the presence of some smectite, vermiculite, and chlorite in the soils. These differences were confirmed by the results determined by the Mg-Eg saturated, K-saturated, and K-550 treatments. The stronger peaks at 1.61 and 1.58 nm in Mg-Eg treatments (Fig. 4b, c, and d) supported the existence of a highly charged and/or weakly crystalline smectite in the soils. The 1.00 and 1.01 nm (001) asymmetric basal reflections in the Mg-saturated treatment indicated the presence of illite in the soil samples. Peaks at 1.06 nm (001) and 0.63 nm (002) indicated the presence of palygorskite, which was confirmed by SEM analysis on a few samples (Fig. 5). In addition, the 1.20 nm (001) peak revealed the presence of sepiolite in the soils.

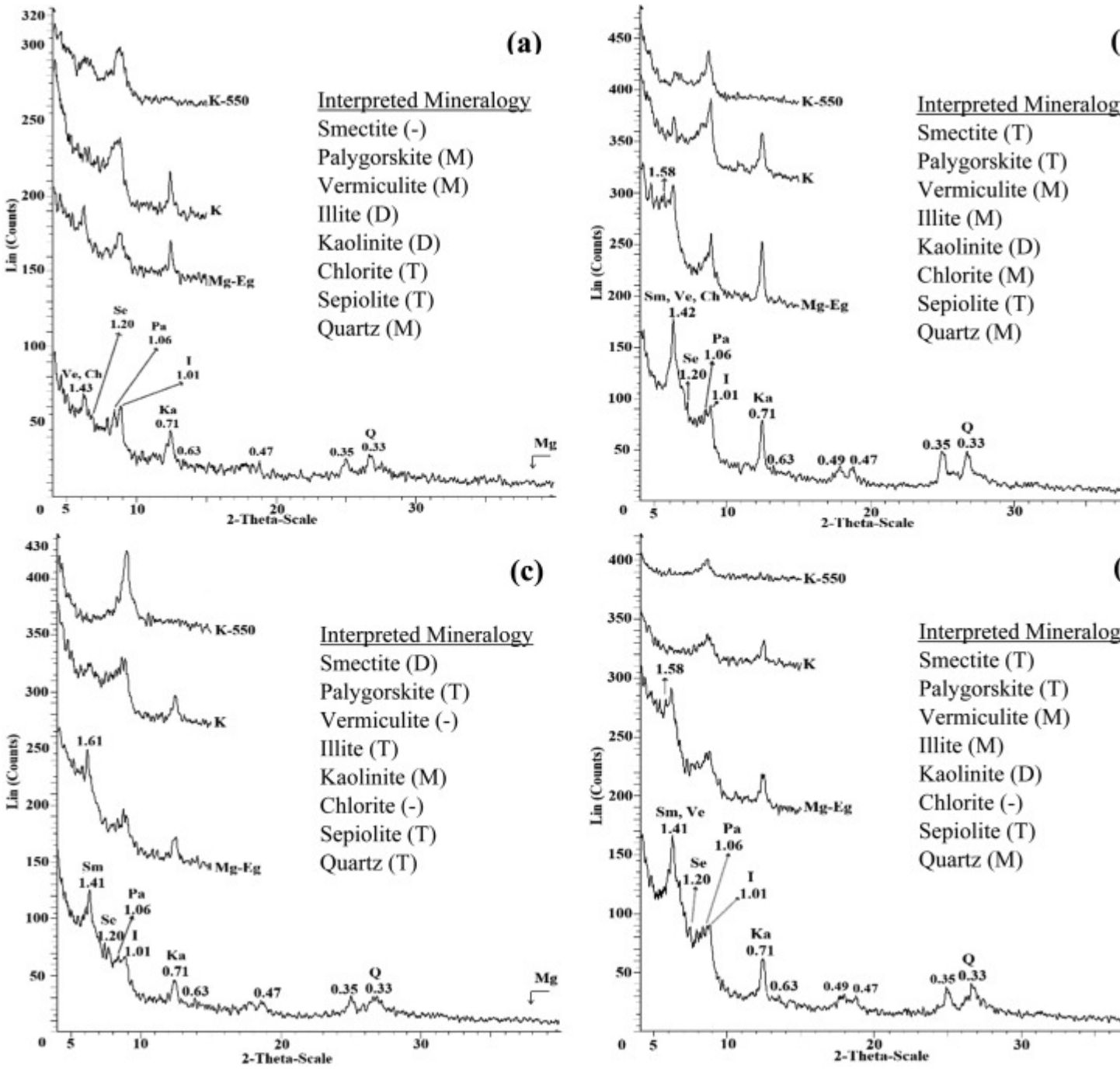

1. Download : Download high-res image (833KB)
2. Download : Download full-size image

Fig. 4. X-ray diffractograms of the clay fraction: a) Bnyz1 horizon of P1; b) Anyz horizon of P2; c) Btnyz horizon of P2; and d) Btnyzg2 horizon of P3. Note: Sm = Smectite; I = Illite; Pa = Palygorskite; Ch = Chlorite; Ka = Kaolinite; Ve = Vermiculite; Se = Sepiolite; Q = Quartz; Magnesium (Mg); Magnesium-Ethylene glycol (Mg-EG); Potassium (K); Potassium-heating (K-

550). In the Interpreted Mineralogy, D = dominant (>25%), M = moderate (10–25%), T = trace (<10%), - = not detected.

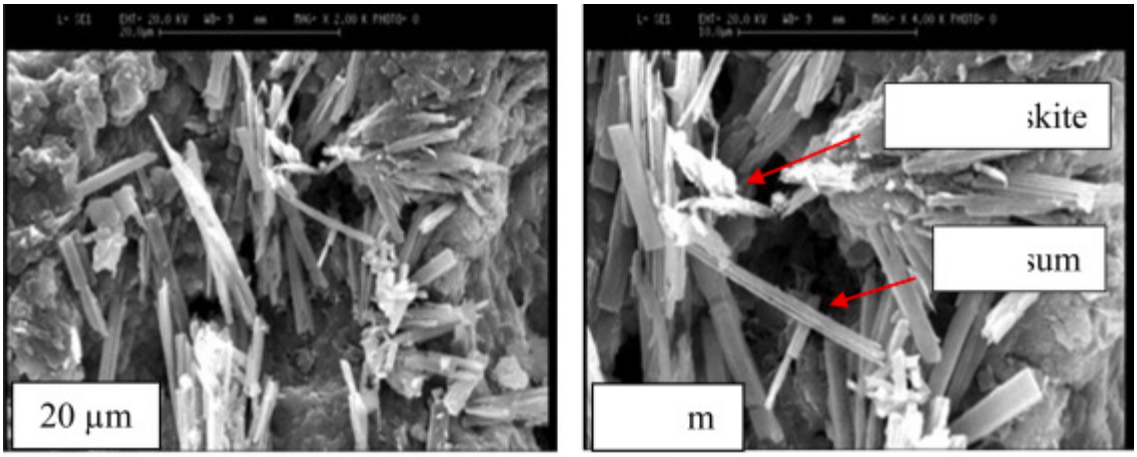

1. Download : Download high-res image (441KB)
2. Download : Download full-size image

Fig. 5. Scanning Electron Microscopy (SEM) of fibrous clay minerals (i.e., palygorskite) in the studied soils.

3.3. Rheological properties

The microstructural elasticity of the studied pedons was inferred from the *integral z* and γ_f parameters that were measured by AST under oscillatory conditions (Table 3). The near-surface A horizons (analyzed at 10 cm depth) had less stable microstructures, with lower *integral z* and γ_f values compared to the subsurface horizons (analyzed at 40 cm depth). P2 had the most notable differences: its Anyz horizon had the smallest values of any horizon, whereas its Btnyz horizon had the largest values with the exception of the quasi-saturated (0 kPa) condition. P3 had substantially less microstructural stability in its Btnyzg2 horizon compared to the subsurface horizons in P1 and P2.

Table 3. Summarized results from amplitude sweep tests (ASTs) with controlled shear deformation for samples at three matric potentials (0, −6, and −15 kPa; n = 3).

Pedon No.	Horizon	0 kPa		-6 kPa		-15 kPa	
		integral z	**γ_f (%)**	***integral z***	**γ_f (%)**	***integral z***	**γ_f (%)**
1	Anz	1.90 ± 0.24	2.26 ± 0.33	3.25 ± 0.25	4.85 ± 0.80	2.78 ± 0.48	3.66 ± 0.63
	Bnyz1	7.76 ± 0.70	8.78 ± 0.91	10.10 ± 1.01	11.71 ± 0.64	13.50 ± 1.36	17.78 ± 1.88
2	Anyz	0.45 ± 0.14	0.44 ± 0.12	0.85 ± 0.07	0.93 ± 0.21	1.26 ± 0.24	1.45 ± 0.26

Pedon No.	Horizon	0 kPa		-6 kPa		-15 kPa	
		integral z	**γ_f (%)**	***integral z***	**γ_f (%)**	***integral z***	**γ_f (%)**
3	Btnyz	4.60 ± 1.09	7.19 ± 0.94	11.42 ± 1.00	15.27 ± 2.13	21.40 ± 1.18	25.96 ± 2.54
	Anz	1.54 ± 0.44	1.71 ± 0.57	4.29 ± 0.65	4.38 ± 1.00	5.33 ± 0.63	5.62 ± 0.59
	Btnyzg2	3.33 ± 1.06	3.53 ± 1.41	6.87 ± 1.03	7.40 ± 0.56	7.25 ± 0.77	8.70 ± 0.55

The integral z parameter quantifies microstructural elasticity and was calculated using Eq. (4); γf represents the deformation at the material flow point.

The AST curves also revealed differences in the rheological characteristics of the studied soil horizons (Fig. 6). For instance, the Btnyz horizon of P2 had a more stable microstructure and greater rigidity compared to the B horizons of P1 and P3, as indicated by a delayed transition to predominantly plastic behavior (i.e., the flow point occurred at a higher strain value; Fig. 6d). The Btnyz horizon in P2 had a clayey texture, whereas the Btnyg2 horizon in P3 had a clay loam texture and the Bnyz1 horizon in P1 had a sandy loam texture. The fine-textured clayey soil, therefore, had great elastic deformation behavior than its coarse-textured counterparts. However, tan δ was nearly constant between $1 < \gamma < 10\%$ in the Bnyz1 horizon of P1 (Fig. 6b), causing that soil to have larger *integral z* and γ_f values than the others during the quasi-saturated (0 kPa) tests (Table 3).

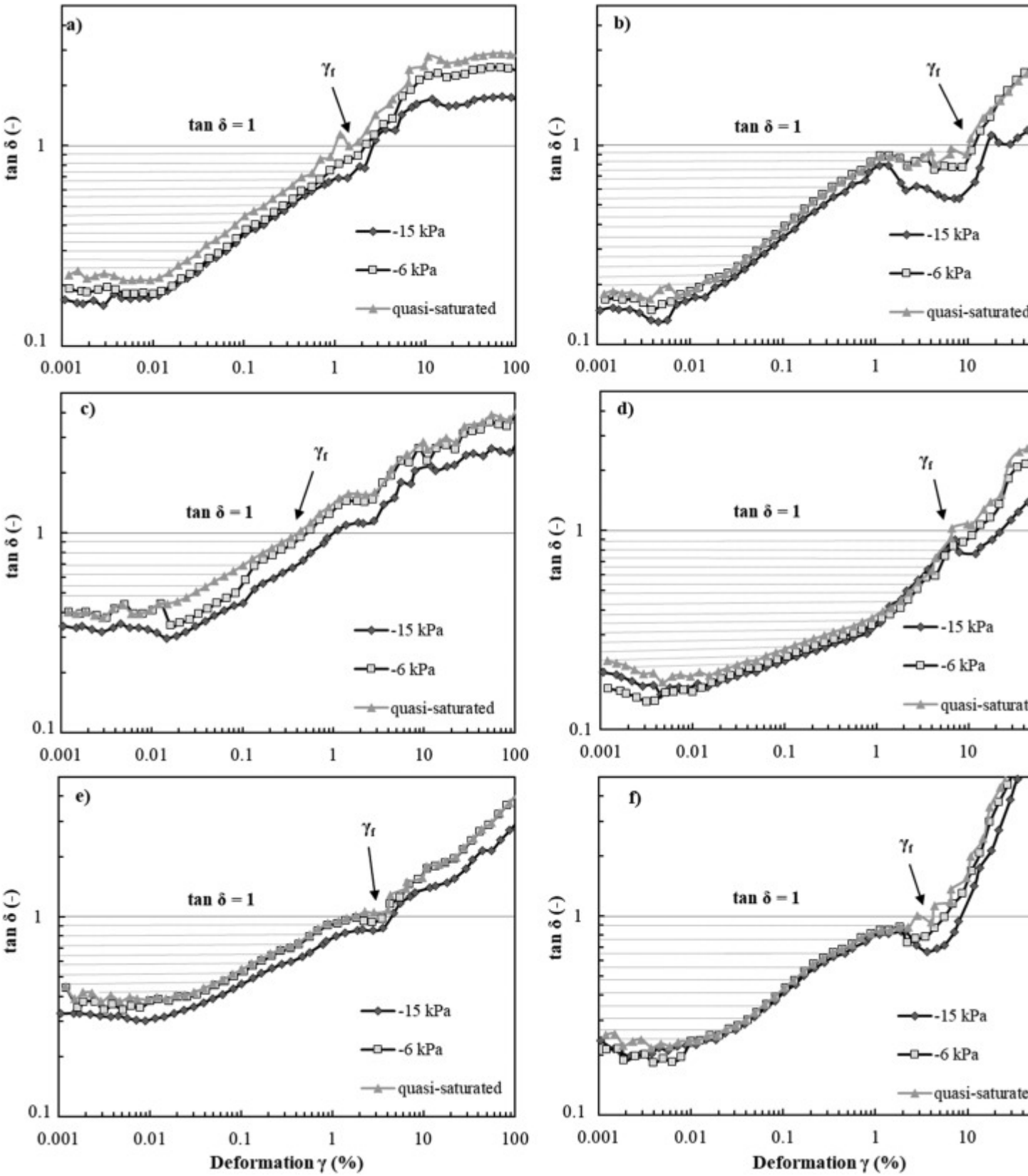

1. Download : Download high-res image (831KB)

2. Download : Download full-size image

Fig. 6. Loss factor (tan δ), derived from amplitude sweep tests under oscillatory conditions and controlled shear deformation for samples prepared at at 0 kPa (quasi-saturated), − 6 kPa, and − 15 kPa matric potentials. a) Anz horizon of P1, b) Bnyz1 horizon of P1, c) Anyz horizon of P2, d) Btnyz horizon of P2, e) Anz horizon of P3, and f) Btnyzg2 horizon of P3. The shaded areas correspond to the integral z parameter and the flow points at 0 kPa are indicated by γf.

3.3.1. Effect of matric potential

Decreasing matric potential of the samples was associated with lower initial values for tan δ, though the differences were more pronounced in the A horizons compared to the B horizons (Fig. 6). In the B horizons, the samples all showed fairly consistent increases in tan δ when deformation was less than 1%. However, once deformation exceeds approximately 1%, tan δ decreased in the samples prepared at − 15 kPa, and only began to increase again once deformation reached 10%. This behavior reflects the re-orientation of the particles into temporarily stable arrangements and a corresponding relative increase in elastic to viscous deformation. The flow point (γ_f) likewise shifted to higher strain values at lower matric potentials (Fig. 6 and Table 3). As a result, *integral z* was larger for samples analyzed under negative matric potentials compared to the quasi-saturated condition, indicating that greater adhesive force between water molecules and solid particles increased the microstructure rigidity.

3.3.2. Correlation coefficients between rheological parameters and soil properties

The correlation analysis, using R/v.2020, revealed significant correlations ($p < 0.01$ and $p < 0.05$) between the two rheological parameters used to indicate microstructural stability: *integral z* and γ_f (Fig. 7). Those parameters were also significantly correlated with CCE and gypsum. At the same time, *integral z* and γ_f values for the three matric potentials (0, −6, −15 kPa) were inversely correlated with EC, SAR, and CROSS, with $-0.5 < r < 0$ for all three parameters. However, these relationships were not significant ($p > 0.05$). Clay content had a strong but not significant correlation with *integral z* and γ_f at − 6 and − 15 kPa ($r > 0.5$; $p > 0.05$).

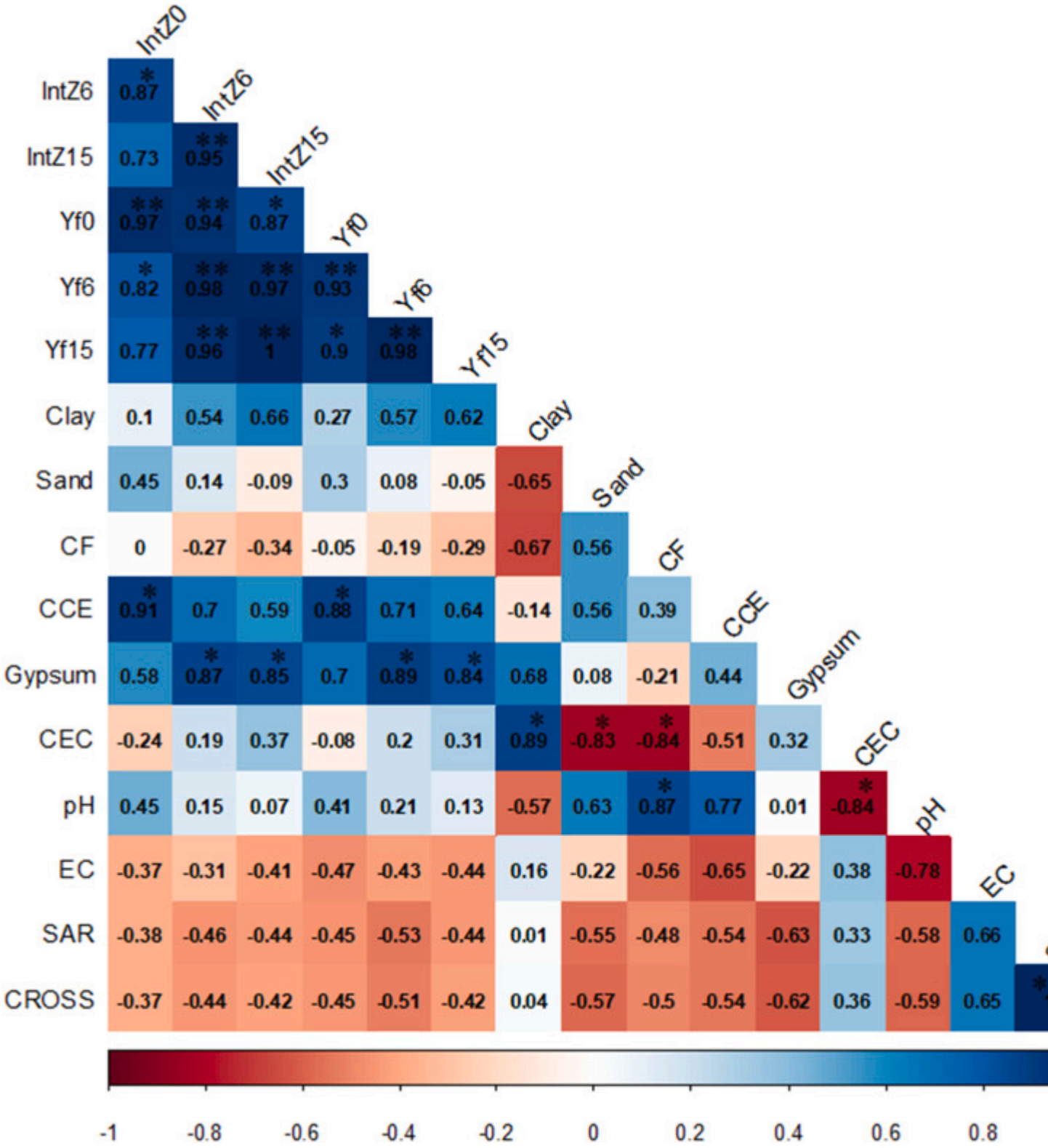

1. Download : Download high-res image (980KB)
2. Download : Download full-size image

Fig. 7. Correlations among integral z at three different matric potentials (0, −6, and −15 kPa) and different studied soil properties. IntZ0 = integral z for samples at a quasi-saturated condition (0 kPa); IntZ6 = integral z for samples at − 6 kPa; IntZ15 = integral z for samples at − 15 kPa; Yf0 = γf for samples at a quasi-saturated condition (0 kPa); Yf6 = γf for samples at − 6 kPa; Yf15 = γf for samples at − 15 kPa; CF = coarse fragments; CCE = calcium carbonate equivalent; CEC = cation exchangeable capacity; EC = electrical conductivity; SAR = sodium adsorption ratio; CROSS = cation ratio of structural stability. * * = significant correlations ($p < 0.01$); * = significant correlations ($p < 0.05$).

The correlation analysis also identified some significant relationships between soil properties. For example, CEC was positively correlated with clay content and negatively correlated with sand content and coarse fragments. SAR and CROSS had a nearly perfect correlation with each other ($r \sim 1$), indicating that the two metrics captured similar information. Further, this correlation indicated that potassium, which is included in CROSS but not SAR, was not an important factor in these soils. The SAR and CROSS values were also positively but not significantly correlated with EC ($r > 0.65$; $p > 0.05$), and were negatively but not significantly correlated with gypsum content ($r < -0.62$; $p > 0.05$). Given the strength of some of these correlations (i.e., $r > 0.6$ or < -0.6), the lack of significant relationships for some of these parameters may reflect the limited number of samples used in the analysis.

4. Discussion

In this study, we characterized the viscoelastic behaviors of saline-sodic soils of Sirjan playa, Iran, using AST measurements. As discussed in the following sections, our analysis indicated that two rheological indicators of microstructural stability, *integral z* and γ_f, both increased as initial matric potential decreased. We also found that soil texture, physicochemical properties, and clay mineralogy were important factors controlling the microstructural stability of these soils.

4.1. Dispersive processes in saline-sodic soils

The values of the *integral z* obtained for the Sirjan playa saline-sodic soils were relatively low (0.45–7.76 for the samples measured under quasi-saturated conditions) compared to those obtained by other authors investigating soil rheology. For example, Markgraf et al. (2012b) and Baumgarten et al. (2013) found *integral z* values of 24–40 in Luvisols and 11–48 in Andosols. The differences are likely attributable to the elevated Na^+ content of our soils compared to those other studies. Further supporting this inference, Stoppe and Horn (2018) determined *integral z* values of 11–61 for fluvial river and sodium-rich marine sediments. Similarly, Batistao et al. (2020) revealed that soils saturated with K^+ had smaller *integral z* values than samples with higher Ca^{2+} and Mg^{2+} content. The presence of monovalent cations, particularly Na^+, increases repellency between soil particles with net negative charges and causes soils to disperse (Rengasamy, 2002, Rengasamy and Marchuk, 2011, Holthusen et al., 2012). Hence, rheological parameters such as γ_f and *integral z* can be useful in evaluating dispersion potential of sodic soils.

In this study, we analyzed our saline-sodic soils at different matric potentials. Our results showed that γ_f and *integral z* increased when the samples had negative matric potentials, with the largest

γ_f and *integral z* values for most horizons occurring at − 15 kPa matric potential. The dewatering of samples that occurred as they dried to − 15 kPa likely increased electrolyte concentrations in the pore space, thus encouraging greater attraction between particles (Stoppe and Horn, 2018). Water menisci that form during dewatering can also provide tension between particles (Ghezzehei and Or, 2001; Laribi et al., 2005; Holthusen et al., 2012; Baumgarten, 2013, Stoppe and Horn, 2018; Khitrov and Khaydapova, 2019). These menisci then encourage inter-particular hydrogel and particle-particle attachment (Pertile et al., 2018; Buchmann et al., 2020).

Soil texture influenced rheological behaviors at different matric potentials. For instance, sand content had a relatively high, though not significant, correlation with *integral z* and γ_f values in the quasi-saturated soils ($r = 0.45$; $p > 0.05$). Conversely, clay content had higher (though not significant) correlations with *integral z* and γ_f under − 6 and − 15 kPa ($r = 0.54$ and 0.66; $p > 0.05$; Fig. 7). In general, clayey soils have greater elastic stability than coarser soils, with shear resistance in saline soils affected by clay content (Mishra et al., 2005).

The relatively sandy Anz horizons in P1 and P3 showed non-linear changes in rigidity when the matric potential changed. Specifically, those soil samples experienced relatively large increases in *integral z* and γ_f between 0 and − 6 kPa, followed by slight decreases between − 6 and − 15 kPa. Sandy soils tend to have large pores that dewater at relatively high matric potentials compared to clayey soils. As a result, the initial water losses in those soils (i.e., when draining to −6 kPa) likely caused water menisci to form between particles and thereby increase soil stability. The continued decrease in matric potential (i.e., to −15 kPa) caused further water loss, meaning that the sandy substrates likely experienced a counterbalancing process between increasing force and decreasing abundance of water menisci (Markgraf and Horn, 2007).

The Anyz horizon at P2 had much less sand than the other two A horizons (18%). In that soil, *integral z* and γ_f both increased by similar magnitudes with each change in matric potential (i.e., between 0 and −6 kPa and between −6 and −15 kPa). This soil layer likely had a wider pore size distributions than the sandier A horizon soils of P1 and P3. Smaller soil pores can hold onto water even as the force associated with the menisci increases (Holthusen et al., 2012), which in our study likely caused the clayey soils to become more rigid as their matric potential decreased.

4.2. Influence of clay minerals

Soil elasticity also varies depending on the type of clay minerals present in the soil (Holthusen et al., 2010). The soils studied here had different amounts of smectite, kaolinite, illite, and palygorskite. The Btnyz horizon of the P2 had more smectite than the other analyzed layers, and also had more shear resistance, as indicated by the relatively high values for γ_f and *integral z*. The other horizons had relatively more illite than smectite, i.e., the Bnyz1 horizon of P1 and the Btnyzg2 horizon of P3. The latter horizons both had lower γ_f and *integral z* values than the Btnyz horizon (P2), suggesting that illite and kaolinite imparted less microstructural stability than smectite.

Previous work has shown that, under conditions of moderate-to-high sodicity, smectite-rich soils resist dispersion better than soils with higher kaolinite and illite content (Suarez, 1981, West et al., 2004; Markgraf et al., 2007). The soils that we studied here had high SAR and CROSS

values, indicating a predominance of sodium cations. At high concentrations, sodium decreases the thickness of the electric diffuse layer surrounding particles, which reduces the repulsive forces between particles and allows them to flocculate (Luckham and Rossi, 1999). Therefore, at sufficiently high sodium concentrations, smectitic soils become consolidated, which can reduce the volume and tortuosity of cracks (DeCarlo and Shokri, 2014, Wang et al., 2021). In our study, the Anyz versus Btnyz horizons of P2 provided contrasts in smectite content (trace amounts for the A horizon versus dominant amounts in the B horizon) and in microstructural stability, as the A horizon had the lowest *integral z* and γ_f values of all analyzed horizons and the subsurface B horizon had the highest values. These results emphasize how smectite particles can impart structural stability in highly sodic soils.

The stability of kaolinitic and illitic soils are also sensitive to sodium concentrations. At low to moderate concentrations, increasing sodium content reduces soil shear strength in dispersed kaolinites (Warkentin and Yong, 1962). At higher sodium concentrations (e.g., > 0.1 mol Na^+ L^{-1}), reduced repulsive force in the electric diffuse layer allow kaolinite particles to orient themselves in relatively strong face-to-face arrangements (Palomino and Santamarina, 2005), similar to smectites. However, the low charge density of those particles means that, even when flocculated, they may still behave as a single-grained material when exposed to shear such as during AST (Oades and Waters, 1991, Markgraf and Horn, 2007). Single grains have less micro-structural stability than more coherent structures such as microaggregates, as indicated by smaller values for rheological properties (Markgraf and Horn, 2007). Likewise, saline-illitic soils are more easily dispersed than their smectitic counterparts (Laribi et al., 2005). These particles have terraced surfaces that can lead to mismatches between faces and smaller attractive forces when the particles come into close proximity with one another (Oster, 1982). As a result, illite- and kaolinite-rich soils both experience more dispersion than soils with higher smectite content, thus explaining some of the differences in rheological parameters observed in our study.

Our X-ray diffraction and SEM measurements also revealed the presence of fibrous clay minerals, including palygorskite and sepiolite, in the soils of Sirjan playa. Palygorskite was most abundant in the Bnyz1 horizon of P1. Even though this soil had high amounts of illite and kaolinite, it possessed the second largest values for *integral z* and γ_f (behind only the Btnyz horizon of P2). Therefore, it is likely that the the presence of palygorskite improved resistance to slaking and dispersion in that soil. Previous work has suggested that rheological parameters such as *integral z* and γ_f increase with the length/width ratio of individual palygorskite fibers (Neaman and Singer, 2000). At the same time, when palygorskite enters suspension with salts, floccules form a three-dimensional network of “scaffolding” structures (Van Olphen, Hsu, 1978). These scaffolds become destroyed during the AST tests, which causes the structure to change to parallel-oriented particles (Chemeda et al., 2014). This new orientation tends to have greater stability, which translates to increased shear resistance. A similar process may happen under natural conditions at high sodium contents, as repulsive forces between particles become suppressed by the elevated cation concentration in the electric diffuse layer (Rengasamy and Olsson, 1991, Batistao et al., 2020). In such instances, clay minerals shift from disjointed to stacked arrangements that better resist dispersion (DeCarlo and Shokri, 2014). Therefore, palygorskite may contribute more to microstructural stability in saline soils with high sodium concentrations (i.e., sodic soils).

4.3. Influence of gypsum and calcium carbonate equivalent

In this study, we found strong correlations between microstructural stability (i.e., *integral z* and γ_f) and gypsum and CCE (in the 0 kPa condition), and between microstructural stability and gypsum in the − 6 and − 15 kPa conditions. These results indicate that these minerals likely help to inhibit soil particle dispersivity. Furthermore, gypsum and CCE are sources of calcium in the saline-sodic soils, where Ca^{2+} increases soil structural stability and hydraulic conductivity due to particle flocculation in the presence of divalent cations (Reading et al., 2012, Filho et al., 2020). Though we did not control gypsum addition in this study, some of the studied soils presented high concentrations of gypsum due to their locations near the ancient Sirjan playa lake. In accordance with previously cited studies, these gypsum resources likely counterbalanced the impact of Na^{+}.

These findings resemble those reported in several previous studies. For example, Markgraf et al. (2012a) studied the microstructural changes of saline-sodic soils due to fertilization. The authors found that phospho-gypsum fertilization increased the strength of saline-sodic soils, which allowed for more productive land use. Similarly, Oster (1982) illustrated how net surface charge varied due to mineral dissolution of calcite following gypsum amendment, which may also be occurring in the soils of this study from naturally occurring calcite and gypsum minerals. Finally, Baumgarten et al. (2012) investigated stiffness degradation of saline-sodic tidal soils under semi-arid conditions in Germany, and found decreasing dispersivity and increasing aggregation with more Ca^{2+}. Therefore, gypsum and CCE appear to be reliable parameters for estimating the degree of dispersion and crusting effects in the saline-sodic soils.

In our study, the Solonchaks soil horizons had higher sodium contents and lower microstructural stability than the Solonetz horizons, meaning that the Solonchaks soils would likely be the most affected by erosion and low infiltration. At the same time, many of the agricultural operations in the region also occur on Solonchaks soils (e.g., the pistachio orchards near P1). We therefore recommend that future research should quantify slaking and soil loss processes within this specific soil group. We also suggest that these soils would benefit greatly from more research to evaluate the effectiveness of management practices such as the use of salt-tolerant crops, planting appropriate cover crops to increase soil organic matter, and adding coarse-textured sand particles to soils, which some local farmers have attempted as a way to encourage greater infiltration rates.

5. Conclusions

Oscillatory stress measurements on saline-sodic soils of the Sirjan playa, Iran, indicated relatively low values for flow point (γ_f) and *integral z*, corresponding to poor microstructural stability. We attributed this result to the high concentration of Na^{+}, which created sodic conditions that encourage particle dispersion. However, the effects of sodicity differed among the studied pedons. Soil horizons with higher smectite and palygorskite content tended to have greater microstructural stability, while those with more illite and kaolinite had a greater tendency to disperse. Sufficiently high sodium concentrations in the soil solution may encourage stronger interactions and tighter arrangements among swelling minerals (e.g., smectite) and also among fibrous minerals (e.g., palygorskite). At the same time, shear resistance was lower in coarser-

textured soils than in finer-textured ones, and was higher in subsurface samples than in surface samples. We assumed that these differences were likewise influenced by electrostatic interactions among soil particles: in both comparisons the soil grouping associated with higher charge and reactivity (e.g., higher CEC) had greater microstructural stability.

We performed our rheological measurements with soil samples under three different matric potentials: 0, − 6, and − 15 kPa. Deformation resistance and microstructural stability were greater at lower matric potentials in the saline-sodic soils. Sandier soils had a relatively large increase in microstructural stability during the initial dewatering phase (0 to −6 kPa) and had only a small increase during the second phase (−6 to −15 kPa), which we ascribed to a tradeoff between increasing tension from water menisci and decreasing abundance of water-filled pores. Finer-textured soils had consistent increases in microstructural stability between dewatering phases, likely because the smaller pores of those soils retained water menisci. Our results also showed that CCE had a counterbalancing effect on the presence of high Na^+, and thereby improved the microstructural stiffness for the quasi-saturated samples. Similarly, gypsum content had a significant positive correlation with *integral z* at − 6 and − 15 kPa matric potentials. Therefore, counterions such as carbonate and sulfate can help improve soil stability in saline-sodic soils such as the ones investigated in this study.

Altogether, this study highlights the importance of combining rheological tests, physicochemical measurements, and mineralogical analyses when assessing particle dispersion potential in salt-affected environments. At the same time, the study results emphasize that rheological measurements can identify saline-sodic soils that have strongly degraded microstructural stability and would most benefit from active management and amelioration. This information may be particularly important when working to prevent erosion losses or remediate decreases in soil infiltration capacity.

Declaration of Competing Interest

The authors declare that they have no known competing financial interests or personal relationships that could have appeared to influence the work reported in this paper.

Acknowledgments

We thank the Vali-e-Asr University of Rafsanjan, Iran, and Virginia Tech University, VA, U.S., for providing facilities. Funding for this work was provided in part by the Virginia Agricultural Experiment Station and the Hatch Program of the National Institute of Food and Agriculture, USDA (1026126).

References

Adamczyk and Weroński, 1999

Z. Adamczyk, P. Weroński

Application of the DLVO theory for particle deposition problems

Adv. Colloid Interface Sci., 83 (1–3) (1999), pp. 137-226

Article

Download PDFView Record in ScopusGoogle Scholar

Agassi et al., 1981

M. Agassi, I. Shainberg, J. Morin

Effect of electrolyte concentration and soil sodicity on infiltration rate and crust formation

Soil Sci. Soc. Am. J., 45 (5) (1981), pp. 848-851

CrossRefGoogle Scholar

Ajayi and Horn, 2017

A.E. Ajayi, R. Horn

Biochar-induced changes in soil resilience: effects of soil texture and biochar dosage

Pedosphere, 27 (2) (2017), pp. 236-247

Article

Download PDFView Record in ScopusGoogle Scholar

Batistao et al., 2020

A.C. Batistao, D. Holthusen, J.M. Reichert, J.C. Portela

Soil solution composition affects microstructure of tropical saline alluvial soils in semi-arid environment

Soil Tillage Res., 203 (2020), Article 104662

Article

Download PDFView Record in ScopusGoogle Scholar

Baumgarten, 2013

W. Baumgarten

Soil microstructural stability as influenced by physicochemical parameters and its environmental relevance on multiple scales. Habilitation Thesis

Christ. -Albrechts-Univ. Kiel. (2013)

Google Scholar

Baumgarten et al., 2013

W. Baumgarten, J. Dörner, R. Horn

Microstructural development in volcanic ash soils from South Chile

Soil Tillage Res., 129 (2013), pp. 48-60

Article

Download PDFView Record in ScopusGoogle Scholar

Baumgarten et al., 2012

W. Baumgarten, T. Neugebauer, E. Fuchs, R. Horn

Structural stability of Marshland soils of the riparian zone of the Tidal Elbe River

Soil Tillage Res., 125 (2012), pp. 80-88

Article

Download PDFView Record in ScopusGoogle Scholar

Buchmann et al., 2020

C. Buchmann, Z. Steinmetz, M. Brax, S. Peth, G.E. Schaumann

Effect of matric potential and soil-water-hydrogel interactions on biohydrogel-induced soil microstructural stability

Geoderma, 362 (2020), Article 114142

Article

Download PDFView Record in ScopusGoogle Scholar

Chemeda et al., 2014

Y.C. Chemeda, G.E. Christidis, N.T. Khan, E. Koutsopoulou, V. Hatzistamou, V.C. Kelessidis

Rheological properties of palygorskite–bentonite and sepiolite–bentonite mixed clay suspensions

Appl. Clay Sci., 90 (2014), pp. 165-174

Article

Download PDFView Record in ScopusGoogle Scholar

DeCarlo and Shokri, 2014

K.F. DeCarlo, N. Shokri

Salinity effects on cracking morphology and dynamics in 3-D desiccating clays

Water Resour. Res., 50 (4) (2014), pp. 3052-3072

View Record in ScopusGoogle Scholar

Dixon and Weed, 1989

J.B. Dixon, S.B. Weed

Minerals in soil environments

Soil Science Society of America Inc, (1989)

Google Scholar

Farpoor et al., 2012

M.H. Farpoor, M. Neyestani, M.K. Eghbal, I.E. Borujeni

Soil–geomorphology relationships in Sirjan playa, south central Iran

Geomorphology, 138 (1) (2012), pp. 223-230

Article

Download PDFView Record in ScopusGoogle Scholar

Filho et al., 2020

G.F. Filho, N. da Silva Dias, S.R.P. Suddarth, J.F. Ferreira, R.G. Anderson, C. dos Santos Fernandes, R.B. de Lira, M.F. Neto, C.R. Cosme

Reclaiming Tropical Saline-Sodic Soils with Gypsum and Cow Manure

Water, 12 (57) (2020), pp. 1-13

CrossRefView Record in ScopusGoogle Scholar

Fuchs, 2005

Y. Fuchs

Clays, Economic Uses

R.C. Salley, L.R.M. Cocks, I.R. Plimer (Eds.), Encyclopedia of geology, Academic Press, Elsevier (2005), pp. 366-370

Article

Download PDFGoogle Scholar

Gee and Bauder, 1986

G.W. Gee, J.W. Bauder

Particle-size analysis 1

Methods Soil Anal.: Part 1—Physical Mineral. Methods, (methodsofsoilan1) (1986), pp. 383-411

View Record in ScopusGoogle Scholar

Ghezzehei and Or, 2001

T.A. Ghezzehei, D. Or

Rheological properties of wet soils and clays under steady and oscillatory stresses

Soil Sci. Soc. Am. J., 65 (3) (2001), pp. 624-637

CrossRefView Record in ScopusGoogle Scholar

Han et al., 2019

L. Han, D. Liu, G. Cheng, G. Zhang, L. Wang

Spatial distribution and genesis of salt on the saline playa at Qehan Lake, Inner Mongolia, China

Catena, 177 (2019), pp. 22-30

Article

Download PDFCrossRefView Record in ScopusGoogle Scholar

Holthusen et al., 2020

D. Holthusen, P. Pertile, G.O. Awe, J.M. Reichert

Soil density and oscillation frequency effects on viscoelasticity and shear resistance of subtropical Oxisols with varying clay content

Soil Tillage Res., 203 (2020), Article 104677

Article

Download PDFView Record in ScopusGoogle Scholar

Holthusen et al., 2019

D. Holthusen, P. Pértile, J.M. Reichert, R. Horn

Viscoelasticity and shear resistance at the microscale of naturally structured and homogenized subtropical soils under undefined and defined normal stress conditions

Soil Tillage Res., 191 (2019), pp. 282-293

Article

Download PDFView Record in ScopusGoogle Scholar

Holthusen et al., 2010

D. Holthusen, S. Peth, R. Horn

Impact of potassium concentration and matric potential on soil stability derived from rheological parameters

Soil Tillage Res., 111 (1) (2010), pp. 75-85

Article

Download PDFView Record in ScopusGoogle Scholar

Holthusen et al., 2012

D. Holthusen, D. Reeb, R. Horn

Influence of potassium fertilization, water and salt stress, and their interference on rheological soil parameters in planted containers

Soil Tillage Res., 125 (2012), pp. 72-79

Article

Download PDFView Record in ScopusGoogle Scholar

IUSS Working Group WRB., 2015

IUSS Working Group WRB

World Reference Base for Soil Resources 2014, update 2015

International Soil Classification System for Naming Soils and Creating Legends for Soil Maps. World Soil Resources Reports No. 106. FAO, Rome.Jackson, M. L. 1958, 498, Soil chemical analysis prentice Hall,, Inc., Englewood Cliffs, NJ (2015), pp. 183-204

World Reference Base for Soil Resources 2014, update 2015

Jackson, 1958

M.L. Jackson

Soil Chem. Anal. Prentice. Hall. Inc., Englewood Cliffs, NJ, 498 (1958), pp. 183-204

View Record in Scopus

Javaheri et al., 2021

F. Javaheri, I. Esfandiarpour-Boroujeni, H. Kourki, M.H. Farpoor, R.D. Stewart

Rheological evaluation of soil aggregate microstructure and stability across a forested catena

Geoderma, 403 (2021), Article 115196

Article

Download PDFView Record in ScopusGoogle Scholar

Khitrov and Khaydapova, 2019

N.B. Khitrov, D.D. Khaydapova

Viscoelastic Behavior of Vertic Solonetz in the Kamennaya Steppe

Eurasia Soil Sci., 52 (7) (2019), pp. 808-821

CrossRefView Record in ScopusGoogle Scholar

Kittrick and Hope, 1963

J.A. Kittrick, E.W. Hope

A procedure for the particle-size separation of soils for X-ray diffraction analysis

Soil Sci., 96 (5) (1963), pp. 319-325

CrossRefView Record in ScopusGoogle Scholar

Kottek et al., 2006

M. Kottek, J. Grieser, C. Beck, B. Rudolf, F. Rubel

World map of the Köppen-Geiger climate classification updated

Meteorol. Z., 15 (3) (2006), pp. 259-263

CrossRefView Record in ScopusGoogle Scholar

Krinsley, 1970

D.B. Krinsley

A geomorphological and paleoclimatological study of the playas of Iran. Geological Survey U.S. Department of Interior

Wash. D. C. (1970), p. 486

Google Scholar

Laribi et al., 2005

S. Laribi, J.M. Fleureau, J.L. Grossiord, N. Kbir-Ariguib

Comparative yield stress determination for pure and interstratified smectite clays

Rheol. Acta, 44 (3) (2005), pp. 262-269

View Record in ScopusGoogle Scholar

Liu et al., 2017

Y.L. Liu, S.H. Yao, X.Z. Han, B. Zhang, S.A. Banwart

Soil mineralogy changes with different agricultural practices during 8-year soil development from the parent material of a Mollisol

Adv. Agron., 142 (2017), pp. 143-179

Article

Download PDFView Record in ScopusGoogle Scholar

Luckham and Rossi, 1999

P.F. Luckham, S. Rossi

The colloidal and rheological properties of bentonite suspensions

Adv. Colloid Interface Sci., 82 (1–3) (1999), pp. 43-92

Article

Download PDFView Record in ScopusGoogle Scholar

Markgraf and Horn, 2007

W. Markgraf, R. Horn

Scanning electron microscopy–energy dispersive scan analyses and rheological investigations of South-Brazilian soils

Soil Sci. Soc. Am. J., 71 (3) (2007), pp. 851-859

CrossRefView Record in ScopusGoogle Scholar

Markgraf et al., 2009

W. Markgraf, R. Horn, L. Gragg, J. Cassell

Rheological investigations in soil micro mechanics: measuring stiffness degradation and structural stability on a particle scale

Progress in management engineering, Nova Science Publishers,, New York (2009), pp. 237-279

View Record in ScopusGoogle Scholar

Markgraf et al., 2006

W. Markgraf, R. Horn, S. Peth

An approach to rheometry in soil mechanics—Structural changes in bentonite, clayey and silty soils

Soil Tillage Res., 91 (1–2) (2006), pp. 1-14

Article

Download PDFView Record in ScopusGoogle Scholar

Markgraf et al., 2012a

W. Markgraf, F. Moreno, R. Horn

Quantification of microstructural changes in Salorthidic Fluvaquents using rheological and particle charge techniques

Vadose Zone J., 11 (1) (2012), 10.2136/vzj2011.0061

Google Scholar

Markgraf et al., 2012b

W. Markgraf, C.W. Watts, W.R. Whalley, T. Hrkac, R. Horn

Influence of organic matter on rheological properties of soil

Appl. Clay Sci., 64 (2012), pp. 25-33

Article

Download PDFView Record in ScopusGoogle Scholar

Mezger, 2006

Mezger, T. 2006. The rheology handbook: for users of rotational and oscillatory rheometers. Vincentz Network, Hannover.

Google Scholar

Mezger, 2020

T. Mezger

The rheology handbook: for users of rotational and oscillatory rheometers

Eur. Coat. (2020)

Google Scholar

Mishra et al., 2005

A.K. Mishra, M. Ohtsubo, L. Li, T. Higashi

Effect of salt concentrations on the permeability and compressibility of soil-bentonite mixtures

J. Fac. Agric., Kyushu Univ., 50 (2) (2005), pp. 837-849

CrossRefView Record in ScopusGoogle Scholar

Missana and Adell, 2000

T. Missana, A. Adell

On the applicability of DLVO theory to the prediction of clay colloids stability

J. Colloid Interface Sci., 230 (1) (2000), pp. 150-156

Article

Download PDFView Record in ScopusGoogle Scholar

Neaman and Singer, 2000

A. Neaman, A. Singer

Rheological properties of aqueous suspensions of palygorskite

Soil Sci. Soc. Am. J., 64 (1) (2000), pp. 427-436

CrossRefView Record in ScopusGoogle Scholar

Nelson and Sommers, 1982

Nelson, D.W., Sommers, L.E., 1982. Total Carbon, Organic matter. In: Page, A.L., et al. (Ed.), Method of Soil Analysis. Part II. 2nd ed., Agron. Monger. No. 9. ASA and SSSA, Madison, WI, 539–577.

Google Scholar

Ni and Huang, 2020

H. Ni, Y. Huang

Rheological study on influence of mineral composition on viscoelastic properties of clay

Appl. Clay Sci., 187 (2020), Article 105493

Article

Download PDFView Record in ScopusGoogle Scholar

Oades and Waters, 1991

J.M. Oades, A.G. Waters

Aggregate hierarchy in soils

Soil Res., 29 (6) (1991), pp. 815-828

CrossRefGoogle Scholar

Oster, 1982

J.D. Oster

Gypsum usage in irrigated agriculture: a review

Fertil. Res., 3 (1) (1982), pp. 73-89

View Record in ScopusGoogle Scholar

Palomino and Santamarina, 2005

A.M. Palomino, J.C. Santamarina

Fabric map for kaolinite: effects of pH and ionic concentration on behavior

Clays Clay Miner., 53 (3) (2005), pp. 211-223

View Record in ScopusGoogle Scholar

Pertile et al., 2018

P. Pertile, D. Holthusen, P.I. Gubiani, J.M. Reichert

Microstructural strength of four subtropical soils evaluated by rheometry: properties, difficulties and opportunities

Sci. Agric., 75 (2) (2018), pp. 154-162

CrossRefView Record in ScopusGoogle Scholar

Qadir et al., 2006

M. Qadir, A.D. Noble, S. Schubert, R.J. Thomas, A. Arslan

Sodicity-induced land degradation and its sustainable management: Problems and prospects

Land Degrad. Dev., 17 (6) (2006), pp. 661-676

CrossRefView Record in ScopusGoogle Scholar

Qadir and Schubert, 2002

M. Qadir, S. Schubert

Degradation processes and nutrient constraints in sodic soils

Land Degrad. Dev., 13 (4) (2002), pp. 275-294

View Record in ScopusGoogle Scholar

Quirk and Murray, 1991

J.P. Quirk, R.S. Murray

Towards a model for soil structural behavior

Soil Res., 29 (6) (1991), pp. 829-867

View Record in ScopusGoogle Scholar

Rayment and Higginson, 1992

G.E. Rayment, F.R. Higginson

Australian laboratory handbook of soil and water chemical methods

Inkata Press Pty Ltd (1992)

Google Scholar

Reading et al., 2012

L.P. Reading, T. Baumgartl, K.L. Bristow, D.A. Lockington

Hydraulic conductivity increases in a sodic clay soil in response to gypsum applications: Impacts of bulk density and cation exchange

Soil Sci., 177 (3) (2012), pp. 165-171

View Record in ScopusGoogle Scholar

Rengasamy, 2002

P. Rengasamy

Transient salinity and subsoil constraints to dryland farming in Australian sodic soils: an overview

Aust. J. Exp. Agric., 42 (3) (2002), pp. 351-361

View Record in ScopusGoogle Scholar

Rengasamy and Marchuk, 2011

P. Rengasamy, A. Marchuk

Cation ratio of soil structural stability (CROSS)

Soil Res., 49 (3) (2011), pp. 280-285

View Record in ScopusGoogle Scholar

Rengasamy and Olsson, 1991

P. Rengasamy, K.A. Olsson

Sodicity and soil structure

Soil Res., 29 (6) (1991), pp. 935-952

View Record in ScopusGoogle Scholar

Richards, 1954

L.A. Richards

Diagn. Improv. Saline Alkali Soils, Vol. 78 (No. 2) (1954), p. 154

CrossRefView Record in Scopus

Schoeneberger et al., 2012

P.J. Schoeneberger, D.A. Wysocki, E.C. Benham

Soil Survey Staff. 2012. Field book for describing and sampling soils, Version 3.0. Natural Resources Conservation Service

Natl. Soil Surv. Cent., Linc., NE (2012), pp. 9-14

View Record in ScopusGoogle Scholar

Shainberg et al., 1981

I. Shainberg, J.D. Rhoades, R.J. Prather

Effect of low electrolyte concentration on clay dispersion and hydraulic conductivity of a sodic soil

Soil Sci. NSociety Am. J., 45 (2) (1981), pp. 273-277

CrossRefGoogle Scholar

Smith, 1977

G.I. Smith

Playas and dried lakes: occurrence and development

Quat. Res., 7 (1) (1977), pp. 145-146

Article

Download PDFCrossRefView Record in ScopusGoogle Scholar

Stoppe and Horn, 2018

N. Stoppe, R. Horn

Microstructural strength of tidal soils–a rheometric approach to develop pedotransfer functions

J. Hydrol. Hydromech., 66 (1) (2018), pp. 87-96

CrossRefView Record in ScopusGoogle Scholar

Suarez, 1981

D.L. Suarez

Relation between pHc and sodium adsorption ratio (SAR) and an alternative method of estimating SAR of soil or drainage waters

Soil Sci. Soc. Am. J., 45 (3) (1981), pp. 469-475

CrossRefView Record in ScopusGoogle Scholar

Sumner and Miller, 1996

M.E. Sumner, W.P. Miller

Cation exchange capacity and exchange coefficients

Methods Soil Anal. Part 3—Chemical Methods (1996), pp. 1201-1229

View Record in ScopusGoogle Scholar

Swenson et al., 2002

J. Swenson, R. Bergman, D.T. Bowron, S. Longeville

Water structure and dynamics in a fully hydrated sodium vermiculite clay

Philos. Mag. B, 82 (4) (2002), pp. 497-506

CrossRefView Record in ScopusGoogle Scholar

Torrance, 1999

J.K. Torrance

Physical, chemical and mineralogical influences on the rheology of remoulded low-activity sensitive marine clay

Appl. Clay Sci., 14 (4) (1999), pp. 199-223

Article

Download PDFView Record in ScopusGoogle Scholar

Van Olphen and Hsu, 1978

H. Van Olphen, P.H. Hsu

An introduction to clay colloid chemistry

Soil Sci., 126 (1) (1978), p. 59

CrossRefView Record in ScopusGoogle Scholar

Wang et al., 2021

C. Wang, G. Feng, Z. Zhang, M. Huang, W. Qi, L. Ma

Geometrical and statistical analysis of dynamic crack morphology in shrink-swell soils with addition of maize roots or salinity (NaCl)

Soil Tillage Res., 212 (2021), Article 105057

Article

Download PDFView Record in ScopusGoogle Scholar

Warkentin and Yong, 1962

B.P. Warkentin, R.N. Yong

Shear strength of montmorillonite and kaolinite related to interparticle forces

Clays Clay Miner., 9 (1962), pp. 210-218

Article

Download PDFView Record in ScopusGoogle Scholar

West et al., 2004

S.L. West, G.N. White, Y. Deng, K.J. McInnes, A.S.R. Juo, J.B. Dixon

Kaolinite, halloysite, and iron oxide influence on physical behavior of formulated soils

Soil Sci. Soc. Am. J., 68 (4) (2004), pp. 1452-1460

CrossRefView Record in ScopusGoogle Scholar

Figures

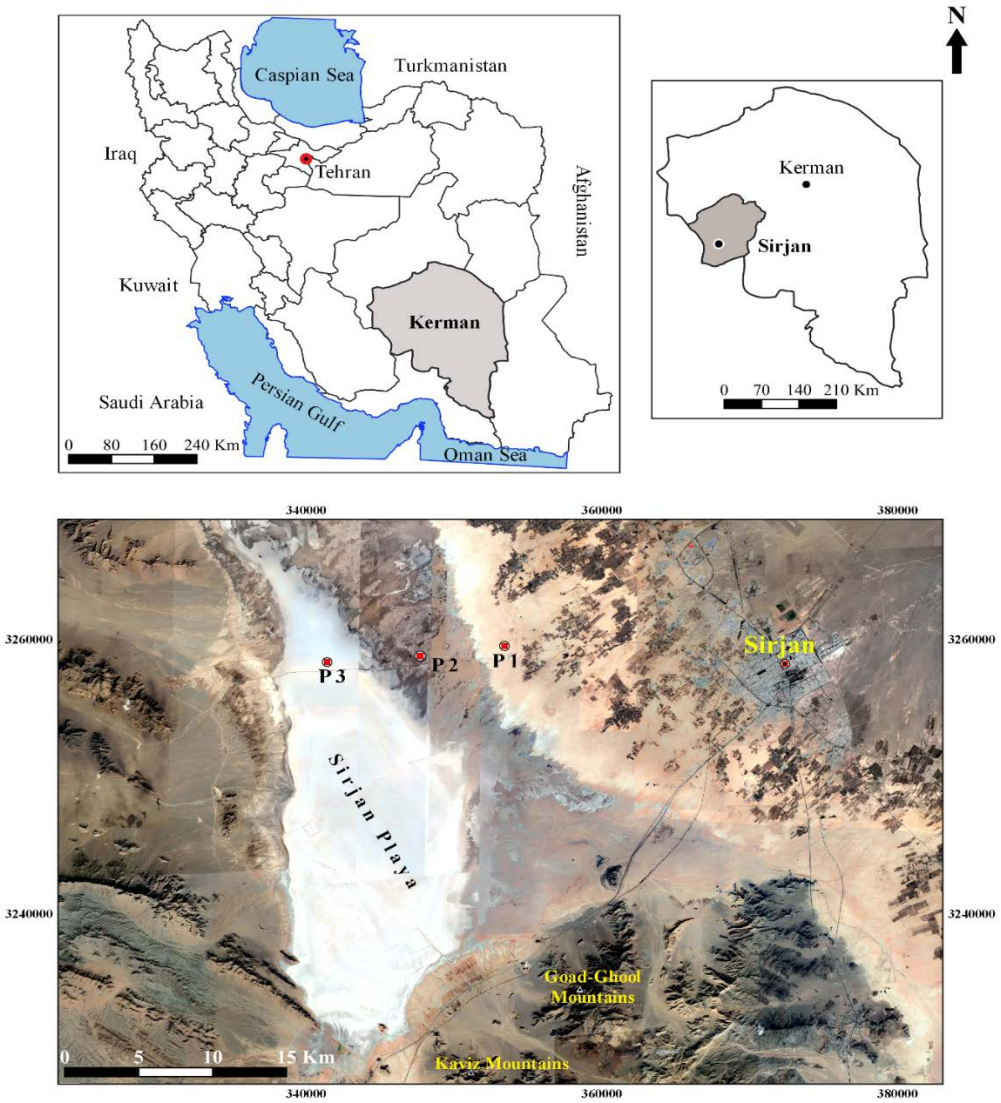

Fig. 1. Location of the study area (top) and the representative pedons (bottom).

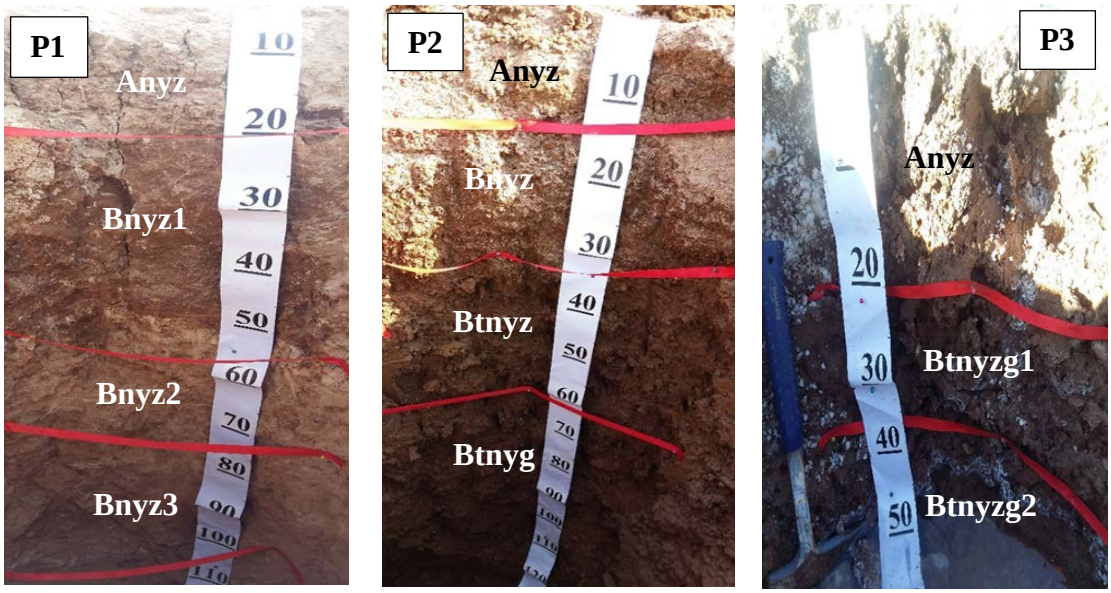

Fig. 2. View of the studied pedons (P1 = Pedon 1; P2 = Pedon 2; P3 = Pedon 3)

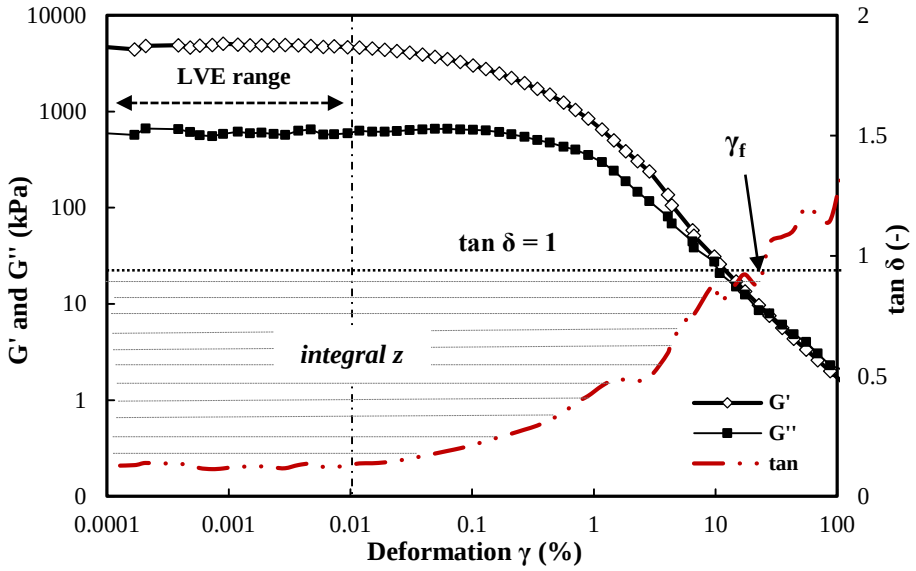

Fig. 3. Example of an amplitude sweep test (AST) result showing G′ (storage modulus) and G″ (loss modulus) as functions of deformation, γ. The loss factor, tan δ, equals $^{G''}/_{G'}$. The *integral z* parameter is calculated as the area between tan δ and 1. The quasi-elastic stage is defined by the linear viscoelastic (LVE) range and derived deformation limit (vertical dashed line). The transition phase between elastic and viscous deformation occurs between the deformation limit and the flow point (γ_f).

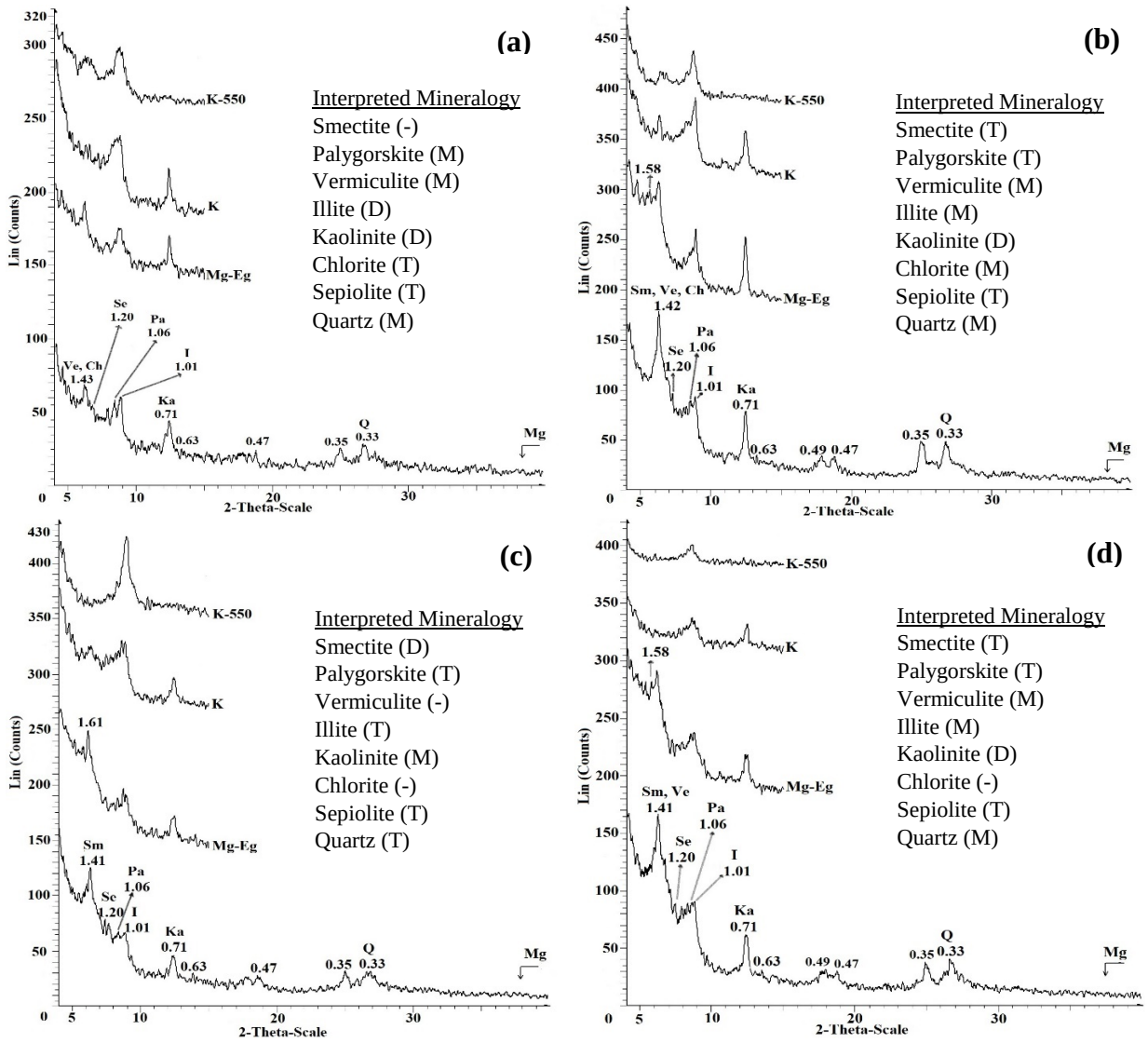

Fig. 4. X-ray diffractograms of the clay fraction: a) Bnyz1 horizon of P1; b) Anyz horizon of P2; c) Btnyz horizon of P2; and d) Btnyzg2 horizon of P3. Note: Sm = Smectite; I = Illite; Pa = Palygorskite; Ch = Chlorite; Ka = Kaolinite; Ve = Vermiculite; Se = Sepiolite; Q = Quartz; Magnesium (Mg); Magnesium-Ethylene glycol (Mg-EG); Potassium (K); Potassium-heating (K-550). In the Interpreted Mineralogy, D = dominant (>25 %), M = moderate (10-25 %), T = trace (<10 %), - = not detected.

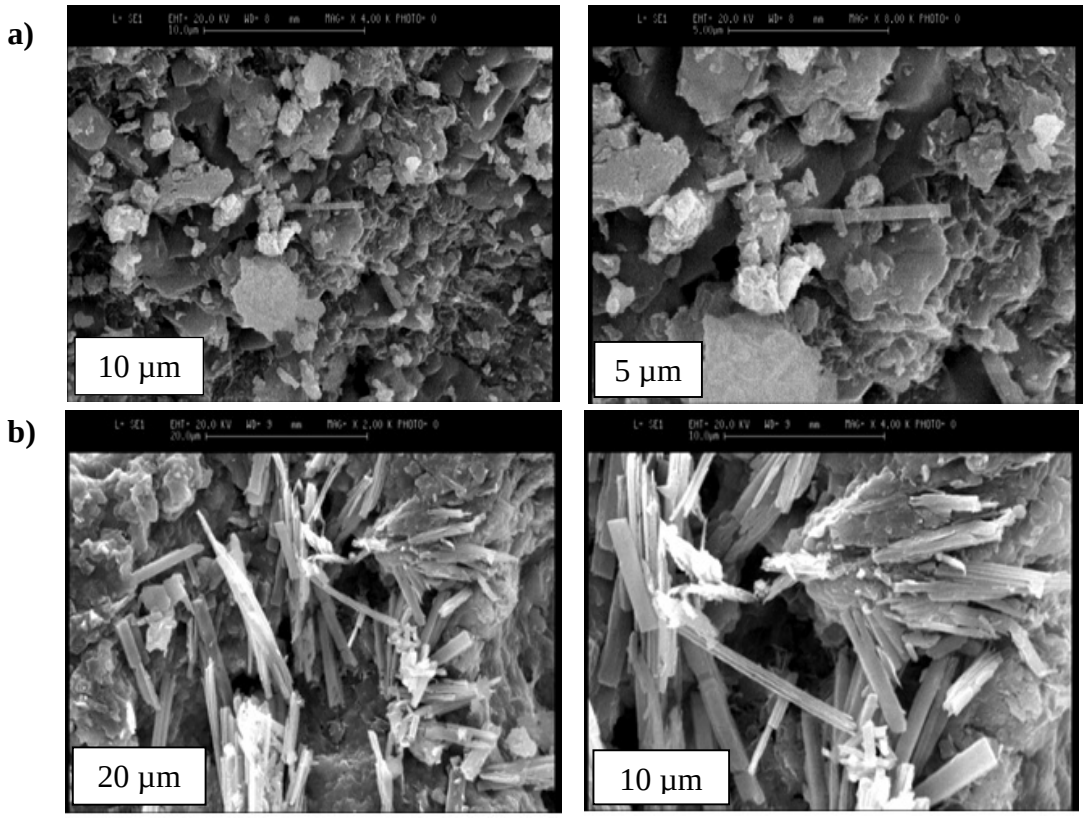

Fig. 5. Scanning Electron Microscopy (SEM) of a) smectites, b) fibrous clay minerals (i.e., palygorskite) in the studied soils.

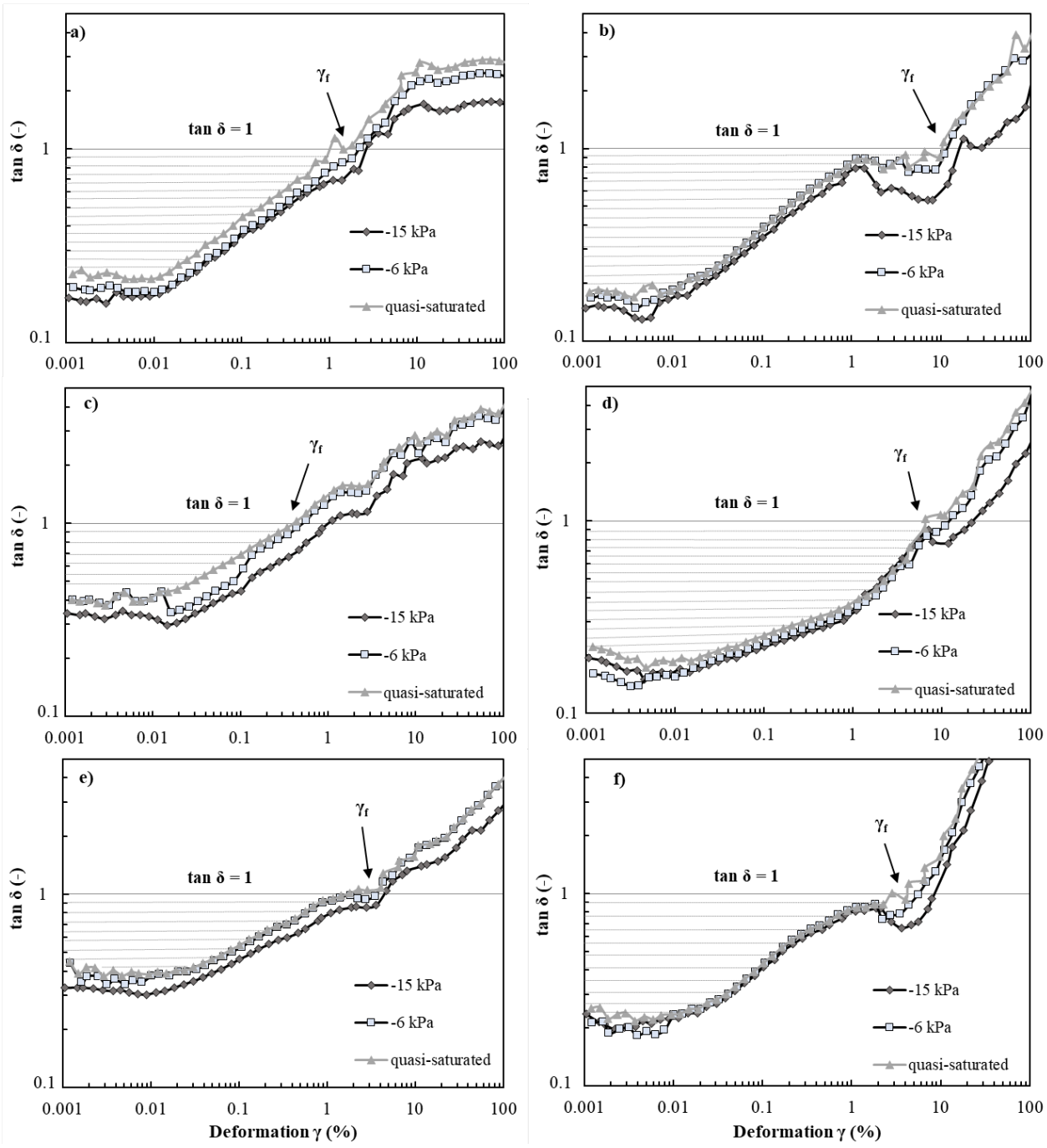

Fig. 6. Loss factor (tan δ), derived from amplitude sweep tests under oscillatory conditions and controlled shear deformation for samples prepared at at 0 kPa (quasi-saturated), -6 kPa, and -15 kPa matric potentials. a) Anz horizon of P1, b) Bnyz1 horizon of P1, c) Anyz horizon of P2, d) Btnyz horizon of P2, e) Anz horizon of P3, and f) Btnyzg2 horizon of P3. The shaded areas correspond to the *integral z* parameter and the flow points at 0 kPa are indicated by γ_f.

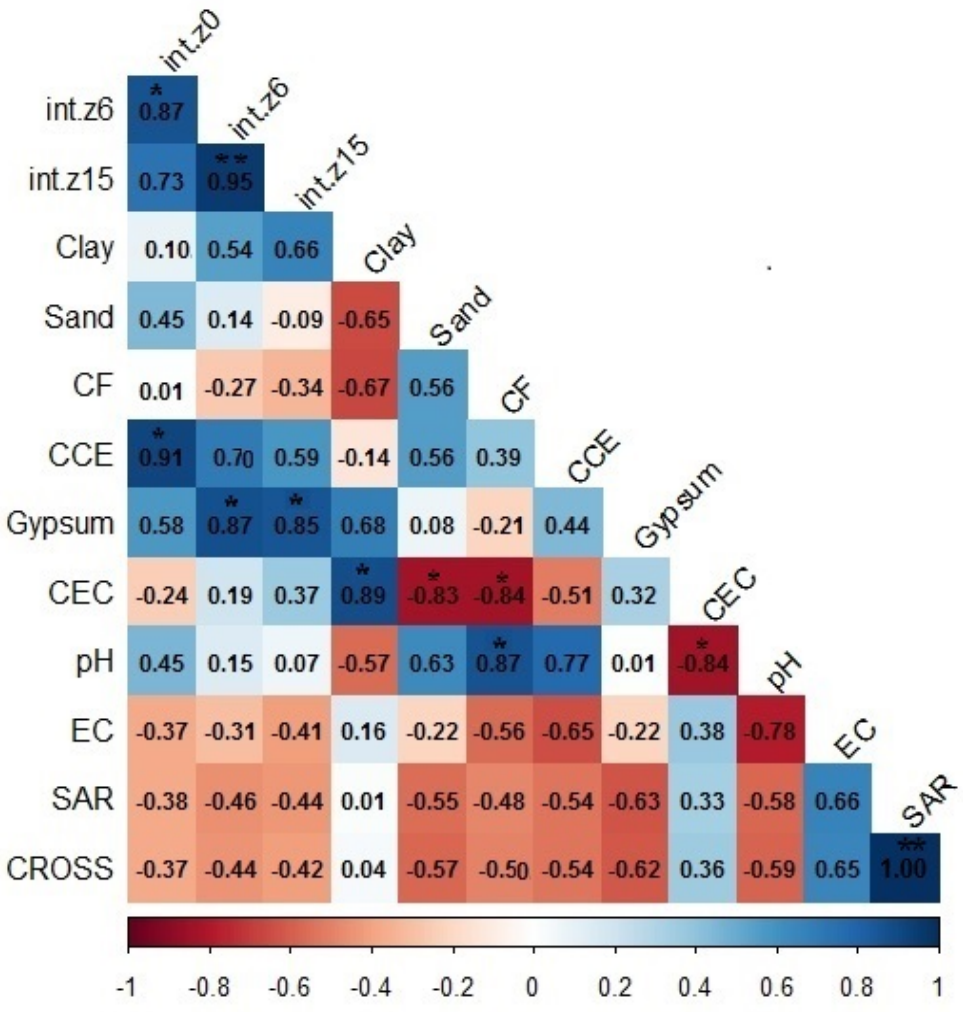

Fig. 7. Correlations among *integral z* at three different matric potentials (0, -6, and -15 kPa) and different studied soil properties. Int.z0 = *integral z* for samples at a quasi-saturated condition (0 kPa); Int.z6 = *integral z* for samples at -6 kPa; Int.z15 = *integral z* for samples at -15 kPa; CF = coarse fragments; CCE = calcium carbonate equivalent; CEC = cation exchangeable capacity; EC = electrical conductivity; SAR = sodium adsorption ratio; CROSS = cation ratio of structural stability. * = significant correlations ($p < 0.05$).

Table 2. Summary of morphological properties of the studied pedons. - = Not detected. ⸸ indicates soil horizons that were analyzed for mineralogy; * indicates soil horizons that were analyzed using the amplitude sweep tests for rheological properties.

Pedon No.	Horizon	Depth (cm)	Boundary[a]	Color		Consistency[b]		SR[c]	Mottles[d]/ Redoximorphic features[e]
				Dry	Moist	Dry	Moist		
Pedon 1: Gypsic Sodic Solonchacks									
1	Anz*	0-21	-	10 YR 5/4	10 YR 4/6	HA	L	pl	-
	Bnyz1⸸*	21-52	V-W	7.5 YR 4/3	7.5 YR 3/3	VH	FI	abk	-
	Bnyz2	52-73	V-W	10 YR 6/3	7.5 YR 4/3	SH	VFR	abk	-
	Bnyz3	73-97	C-S	10 YR 6/4	7.5 YR 4/4	MH	FR	abk	-
	Bnyz4	97-132	C-S	10 YR 6.5/3	7.5 YR 3/2	MH	FR	abk	-
Pedon 2: Gypsic Salic Gleyic Solonetz									
2	Anyz⸸*	0-12	-	7.5 YR 4/3	10 YR 5/6	L	L	pl	-
	Bnyz	12-32	A-W	7.5 YR 3/3	7.5 YR 4/3	L	L	sbk	-
	Btnyz⸸*	32-61	C-S	10 YR 6/3	7.5 YR 3/3	HA	FR	cpr	c, 1, D, 10 Y 6/1, M, S
	Btnyg	61-130	C-S	10 YR 6/3	7.5 YR 3/2	VH	SO	cpr	m, 4, P, 10 Y 6/1, M, S RMX, c, 2, D, 10 Y 6/1, M, I, MAT, L, S
Pedon 3: Gypsic Salic Solonetz									
3	Anz*	0-21	-	10 YR 5/3	10 YR 2/2	L	L	pl	-
	Btnyzg1	21-38	A-W	10 YR 6/3	7.5 YR 3/2	VH	SS	cpr	c, 2, D, 5GY 5/1, M, S
	Btnyzg2⸸*	38-62	C-S	10 YR 6/3	7.5 YR 3/2	VH	SS	cpr	m, 2, P, 5GY 5/1, M, S
	Bzm	62+	C-S	-	-	EH	-	-	-

[a] Boundary: very abrupt (V), abrupt (A), clear (C), smooth (S), wavy (W)
[b] Consistency: Dry: loose (L), slightly hard (SH), moderately hard (MH), hard (HA), very hard (VH), extremely hard (EH); moist: loose (L), very friable (VFR), friable (FR), firm (FI), slightly sticky (SS), non-sticky (SO)
[c] Soil structure (SR): angular blocky (abk), subangular blocky (sbk), platy (pl), columnar (cpr)
[d] Mottles: common (c), m (many), fine (1), medium (2), very coarse (4), distinct (D), prominent (P), moist (M), spherical (S)
[e] Redoximorphic features: reduced matrix (RMX), common (c), medium (2), distinct (D), moist (M), irregular (I), in the matrix (not associated with peds/pores) (MAT), loose (L), sharp (S)

Table 2. Summary of physicochemical properties of the studied pedons. CF = Coarse fragments; CCE = calcium carbonate equivalent; CEC = cation exchange capacity ($cmol_+ kg^{-1}$); SP = saturation percentage; EC = electrical conductivity ($dS\ m^{-1}$); OP = osmotic potential; SAR = sodium adsorption ratio; CROSS = cation ratio of structural stability. ST = soil texture, and C = Clay, L = Loam, CL = Clay Loam, SL = Sandy Loam, SiL = Silt Loam, SCL = Sandy Clay Loam. - = Not detected.

Horizon	Depth (cm)	Clay	Sand	CF	CCE	Gypsum	CEC ($cmol_+ kg^{-1}$)	pH	EC ($dS\ m^{-1}$)	SAR $(mmol\ L^{-1})^{0.5}$	CROSS $(mmol\ L^{-1})^{0.5}$	ST
				(%)								
Pedon 1												
Anz	0-21	18.3	51.0	30.0	9.3	14.6	7.9	7.47	33	75	86	L
Bnyz1	21-52	19.3	58.0	12.4	11.5	16.4	8.3	7.43	48	156	174	SL
Bnyz2	52-73	20.7	64.7	11.9	7.6	26.4	8.6	7.67	70	216	229	SCL
Bnyz3	73-97	17.0	73.0	10.0	7.4	23.2	6.7	7.70	170	456	488	SL
Bnyz4	97-132	14.7	80.7	8.0	7.2	12.5	6.3	7.83	56	232	258	SL
Pedon 2												
Anyz	0-12	25	18.3	5.2	7.5	6.2	19.2	6.71	173	355	393	SiL
Bnyz	12-32	30.7	24.1	2.0	9.4	18.7	23.7	6.83	60	282	335	CL
Btnyz	32-61	50.0	22.0	0.0	9.5	24.3	26.2	6.80	31	113	136	C
Btnyg	61-130	47.7	13.1	0.0	11.5	21.4	21.2	6.88	29	143	164	C
Pedon 3												
Anz	0-21	26.3	44.8	0.0	7.5	14.8	18.7	6.53	220	167	186	L
Btnyzg1	21-38	35.3	40.8	0.0	8.0	17.9	20.4	6.40	317	243	272	CL
Btnyzg2	38-62	38.0	35.0	0.0	8.3	17.9	20.8	6.49	347	271	300	CL
Bzm	62+	-	-	-	-	-	-	-	-	-	-	-

Table 3. Summarized results from amplitude sweep tests (ASTs) with controlled shear deformation for samples at three matric potentials (0, -6, and -15 kPa; n = 3). The *integral z* parameter quantifies microstructural elasticity and was calculated using Eq. (4); γ_f represents the deformation at the material flow point.

Pedon No.	Horizon	0 kPa		-6 kPa		-15 kPa	
		integral z	γ_f (%)	*integral z*	γ_f (%)	*integral z*	γ_f (%)
1	Anz	1.90 ± 0.24	2.26 ± 0.33	3.25 ± 0.25	4.85 ± 0.80	2.78 ± 0.48	3.66 ± 0.63
	Bnyz1	7.76 ± 0.70	8.78 ± 0.91	10.10 ± 1.01	11.71 ± 0.64	13.50 ± 1.36	17.78 ± 1.88
2	Anyz	0.45 ± 0.14	0.44 ± 0.12	0.85 ± 0.07	0.93 ± 0.21	1.26 ± 0.24	1.45 ± 0.26
	Btnyz	4.60 ± 1.09	7.19 ± 0.94	11.42 ± 1.00	15.27 ± 2.13	21.40 ± 1.18	25.96 ± 2.54
3	Anz	1.54 ± 0.44	1.71 ± 0.57	4.29 ± 0.65	4.38 ± 1.00	5.33 ± 0.63	5.62 ± 0.59
	Btnyzg2	3.33 ± 1.06	3.53 ± 1.41	6.87 ± 1.03	7.40 ± 0.56	7.25 ± 0.77	8.70 ± 0.55